Event-by-Event Sensitivity of the STAR-FTPCs Analyzed by Model Comparison

H. Hümmler

Max-Planck-Institut für Physik, München, Germany

Abstract

Predictions from the event generators HIJING, NEXUS and VNI are compared to first characterize the main differences between the models. Then, the fully simulated detector response to input from all three models is compared event by event. The sensitivity of the STAR-FTPCs to event fluctuations of different variables is investigated and suggestions for the future analysis of FTPC data are derived.

This STAR note is based on parts of Holm Hümmler's Ph.D. thesis. The full text of the thesis is available from http://wwwstar.mppmu.mpg.de/Doc/hh_thesis.ps.gz

Chapter 1

Predictions from Different Simulation Models

To study the capability of the detector to distinguish the signals from different physics scenarios, the detector response to simulated events from different models was calculated. Special focus was put on the study of event-wise quantities and their fluctuations. The results of this analysis will follow in chapter 2.

First, the different models will be characterized by the spectra of different particles across the whole phase-space, averaged over a large sample of events. The emphasis is on hadronic signals, as these are the main observables which are accessible to the STAR experiment. Decay products from particle decays within the STAR detector (feeddown) are included in the spectra, so that all particles produced by the model which can, directly or indirectly, cause signals in any part of the detector are counted. On the other hand, this procedure can lead to double-counting. For example, the pionic decay of a charged kaon,

$$K^+ \longrightarrow \pi^+\pi^0 \tag{1.1}$$

within the detector will be counted both as a charged pion and as a charged kaon. In spite of this drawback, this method avoids the dilemma of having to set a limit up to which point decay daughters, rather than parents, are counted. As this chapter focuses on the analysis of model properties, not on any detector performance, the model output is analyzed directly, without the simulation of any detector effects.

To get sufficient statistics, all temperature parameter distributions in the present chapter are mirrored at midrapidity. In the rapidity spectra, this symmetry has not been used. As the spectra should be completely symmetrical, deviations in the presented data can give an impression of the size of the errors.

The basic features of the models used, HIJING, NEXUS and VNI, are as follows:

- **HIJING.** HIJING focuses on the detailed simulation of the early stages of the collision, especially of hard scattering processes, to get the best possible estimate for the production of particles with high transverse momentum (minijets). Colliding nucleons are excited to strings, which are then fragmented using jet production code from elementary particle physics. Soft processes are treated as diffractive scattering or resonance excitation. The space-time development of the collision and reinteractions between the produced particles are not included. As a deconfinement signature, a phenomenological treatment of the suppression of high transverse momentum particles (jet quenching) can be added [Gyu94].

- **NEXUS.** NEXUS focuses on the treatment of soft interactions, also using string theory and thus assuming that there is no deconfinement. Each nucleon is modeled as a composition of partons of varying levels of virtuality, according to the nucleon structure functions measured in deep inelastic electron-nucleon scattering. The hard part of the structure function is treated by perturbative QCD, the soft part as a pseudoparticle called pomeron. All interactions of all structure functions have to add up to the total cross section while at the same time satisfying conservation laws, a problem solved using methods from statistical physics. String fragmentation into hadrons is again done by a mechanism used in jet production. In a second step, the produced hadrons can then perform hadron interactions in vacuum [Dre99].

- **VNI.** VNI treats the nuclear collision completely on the level of quarks and gluons. A parton cascade that includes quantum mechanical features like uncertainty relation smearing traces the development in both space-time and momentum space, treating hard interactions by perturbative QCD and soft interactions by a phenomenological approach. Confinement and deconfinement are done locally by parton coalescence, depending on the space-time evolution. The resulting hadrons and parton clusters are passed on to a hadron-cascade to calculate the development after hadronization [Gei97].

1.1 Pion Spectra

Figure 1.1 shows the number of pions per unit in rapidity per event averaged over a large event sample in intervals of rapidity. Whereas the differences in pion multiplicity within the acceptance of the FTPC ($2.5 <\mid y \mid< 4.0$) are relatively small, there are significant differences around midrapidity, in the acceptance of the TPC. Between HIJING and VNI, the predicted pion production at central rapidities varies by more than a factor of two.

The shapes of the distributions also show differences. In both string models, the pion production extends to the rapidity of the colliding nuclei (at approximately $+/-6$), whereas in VNI, there is no significant pion production beyond a rapidity of $\mid y \mid= 4.5$. Unfortunately, particles in this rapidity region have extremely small angles to the beam pipe, so they are not accessible to any component of the STAR detector. At central rapidities, VNI and NEXUS have a maximum, compared to a plateau, with even slight indications of a minimum, in HIJING. This difference may disappear if medium effects in the form of jet quenching are included in HIJING. The energy loss of high transverse momentum particles in deconfined matter should lead to increased particle production around midrapidity.

The rapidity dependence of the temperature parameters derived from the transverse momentum distributions is shown in figure 1.2. These temperature parameters are calculated by a method first suggested by Hagedorn [Hag65]. In the case of thermodynamically

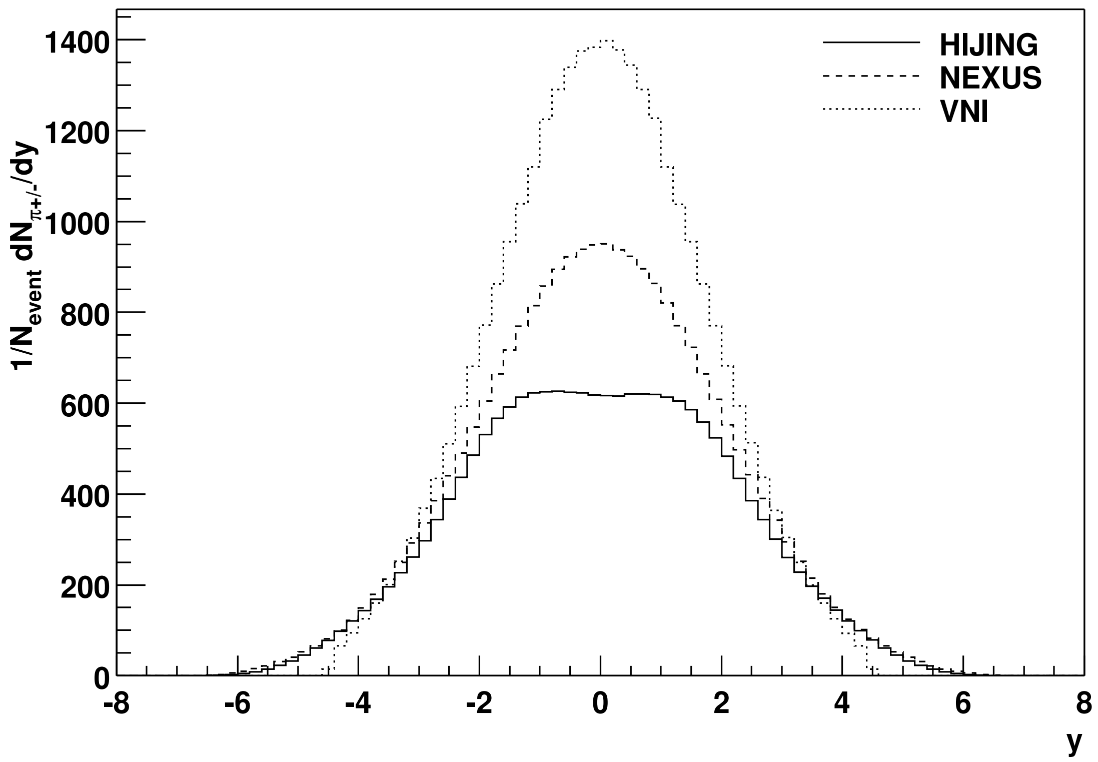

Figure 1.1: *Rapidity distribution of charged pions from three different simulation models. The solid line shows data from HIJING, the dashed line from NEXUS and the dotted line from VNI.*

populated energy states in transverse direction, the transverse mass distribution of the produced particles will have the form

$$\frac{dN}{dm_t^2} \propto const \cdot \exp\left(-\frac{m_t}{T}\right) \tag{1.2}$$

with T having the dimension of a mass or energy. This energy is proportional to the mean kinetic energy (temperature) of the respective particles at the thermal freezeout. An example of a similar distribution can be seen in chapter 2, figure 2.6.

In the present analysis, the temperature parameter was determined by fitting function 1.2 to the experimentally observed particle distribution in a range of m_t corresponding to transverse momenta from $p_t = 300\,\mathrm{MeV/c}$ to $p_t = 1000\,\mathrm{MeV/c}$. Below this range, an enhancement from resonance decay is expected to cause deviations from the exponential spectrum, whereas very high transverse momenta are enhanced by hard parton scattering.

In figure 1.2, both string models show pion temperatures below 200 MeV close to midrapidity and a drop-off at higher rapidities. This behaviour can be explained by energy and momentum conservation in scattering processes, where a particle will usually gain transverse momentum by losing longitudinal momentum.

VNI, on the other hand, yields a much higher pion temperature, which is constant over almost the complete range of rapidity. This is consistent with the thermodynamical model

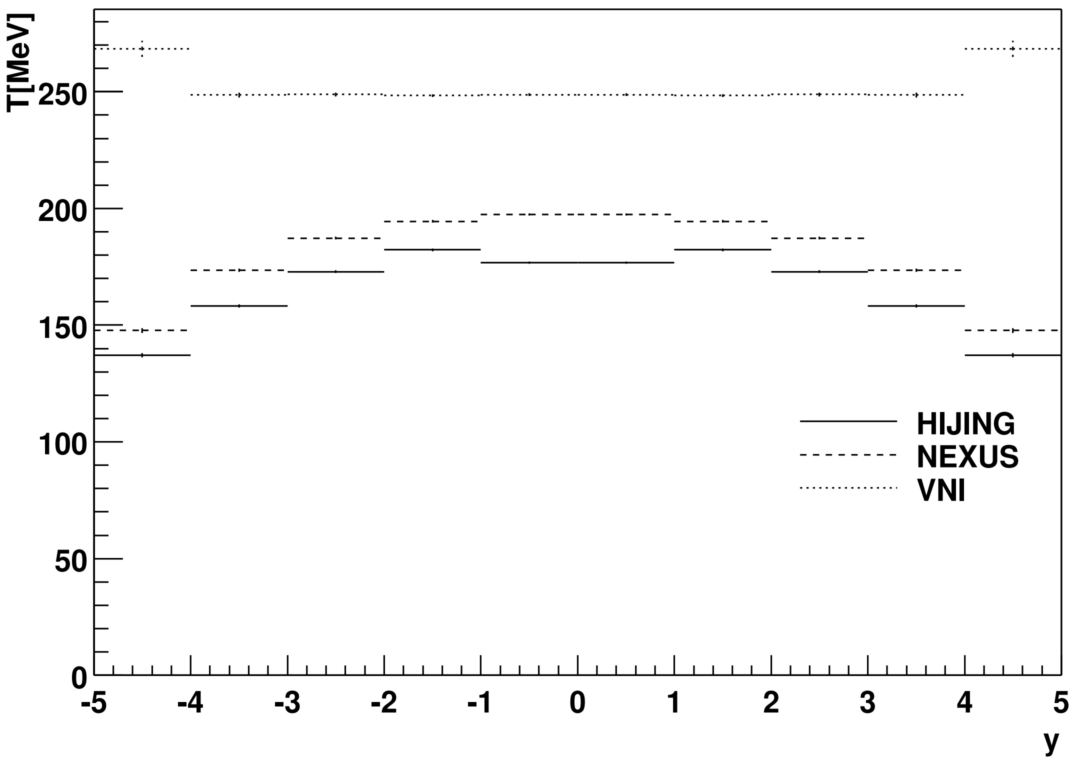

Figure 1.2: *Temperature parameters as functions of rapidity of charged pions from three different simulation models. The solid line shows data from HIJING, the dashed line from NEXUS and the dotted line from VNI. The error bars show only the statistical error from the temperature fit.*

of a longitudinally expanding fireball. In this model, the thermal emission of pions in transverse direction is completely independent of their longitudinal momentum, which is determined by the (ideally boost-invariant) longitudinal expansion of the pion source.

1.2 Kaon Spectra

The kaon rapidity distributions in figure 1.3 show similar shapes as the pions, with a slightly wider distribution from VNI and a slightly narrower one from HIJING. Furthermore, the kaon rapidity distribution from HIJING shows a much clearer minimum at midrapidity. Remarkably, at midrapidity, all three models with their significantly different physics assumptions generate only limited differences in the charged kaon to charged pion ratios of 0.12 for HIJING, 0.15 for NEXUS and 0.16 for VNI. At $y = 3$, however, in the acceptance of the FTPCs, these ratios are 0.11 for HIJING, 0.18 for NEXUS and 0.28 for VNI. Without particle identification, this signal would not be accessible to the FTPC, but the abundance of neutral kaons (which can in principle be reconstructed from the weak decays of K_s^0) should be equal to that of the charged kaons, and the abundance of charged pions can be approximated from the multiplicity of negatively charged particles, so that some information on the K/π ratio can be obtained from FTPC data.

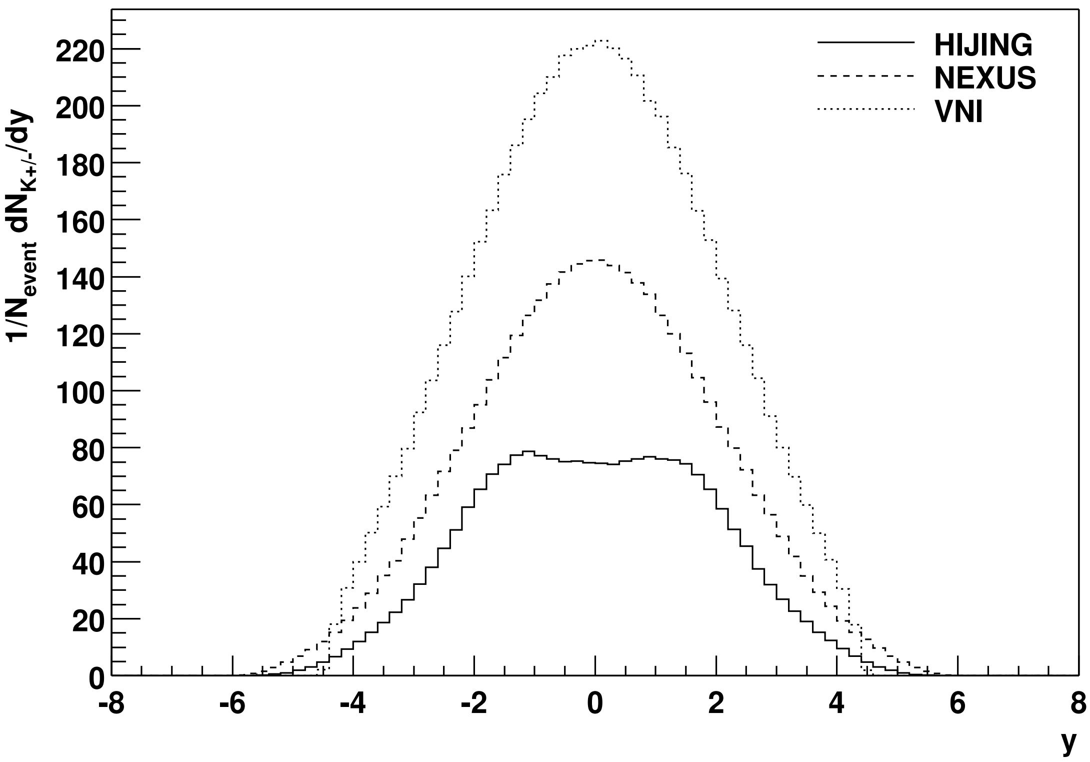

Figure 1.3: *Rapidity distribution of charged kaons from three different simulation models. The solid line shows data from HIJING, the dashed line from NEXUS and the dotted line from VNI.*

The rapidity dependence of kaon temperature parameters in figure 1.4 shows similar systematics as the pion temperatures, at higher levels. In collective models, this increase of average transverse momenta and, thus, measured temperature parameters, is attributed to a collective expansion velocity (radial flow). If the expansion velocity is the same for all particles, its contribution to the momentum will be larger for particles with a higher rest mass. String models should not have flow, but other processes like rescattering or resonance decays may cause different transverse momentum distributions for particles with different mass. This is consistent with the fact that only in VNI the increase in temperature parameters is large enough to be explained by a substantial collective motion.

1.3 Antinucleon Spectra

To eliminate the double-counting of decaying particles, only nucleons (protons and neutrons) and antinucleons are included in the following baryon and antibaryon spectra. This is justified as almost all baryons decay to nucleons within the range of the detector and are counted in this analysis after their decay, avoiding double-counting. This procedure also allows to use the nucleon rest mass to calculate the transverse mass in temperature parameter fits, rather than the mass of every single baryon.

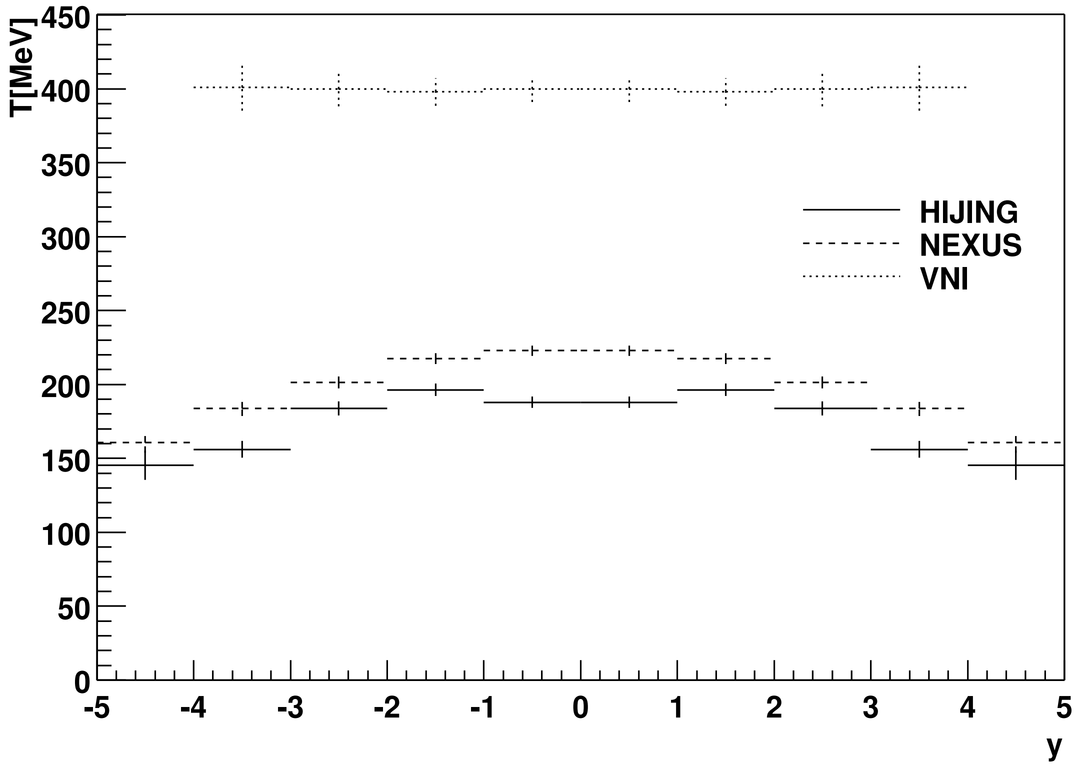

Figure 1.4: *Temperature parameters as functions of rapidity of charged kaons from three different simulation models. The solid line shows data from HIJING, the dashed line from NEXUS and the dotted line from VNI. The error bars show only the statistical error from the temperature fit.*

The antinucleon rapidity distributions in figure 1.5 are generally narrower than the distributions of the lighter particles, probably due to a depletion of antibaryons in the baryon-rich parts of phase-space, at large rapidities. In HIJING, the number of produced antinucleons relative to the number of produced kaons and pions is significantly higher than in the two other models, a fact which may be linked to the small excess of nucleons around midrapidity (see section 1.4). In VNI, on the other hand, the number of antinucleons is relatively small.

The temperature parameters of antinucleons (figure 1.6) in HIJING show only a small increase compared to those of the kaons and pions, a behavior which is to be expected from a string model without rescattering. In both NEXUS and VNI they are significantly higher. In VNI, this is consistent with the kaon data and, thus, with the interpretation as radial flow.

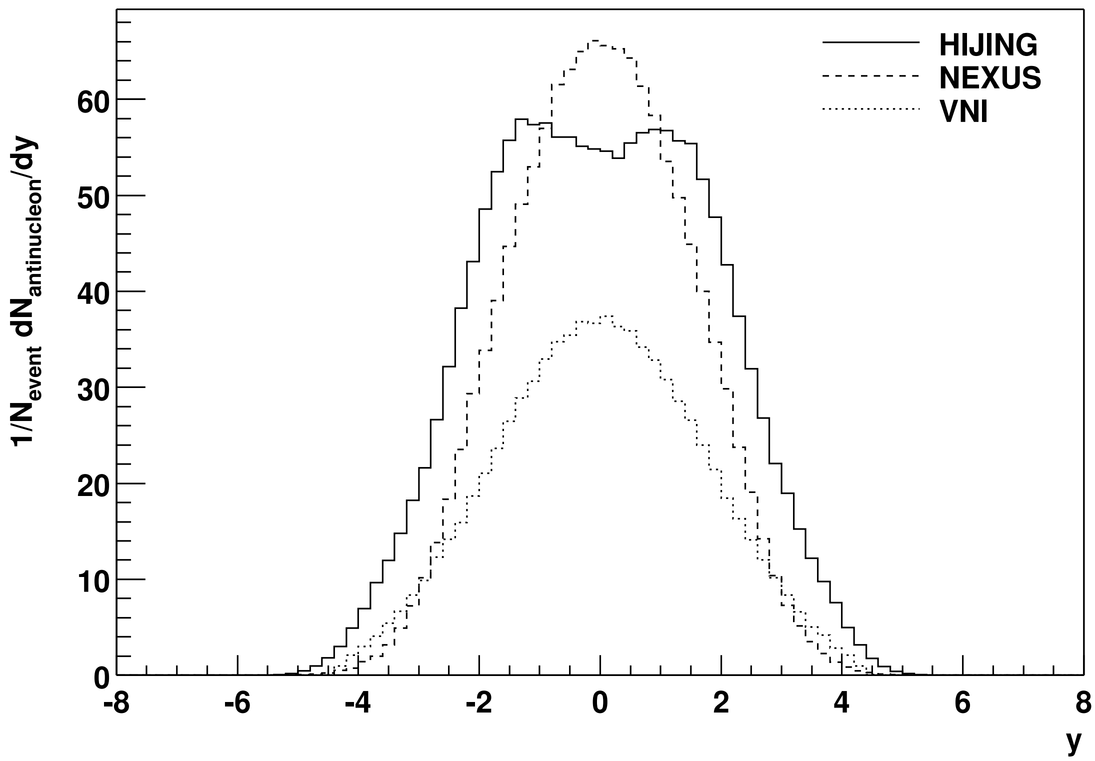

Figure 1.5: *Rapidity distribution of all produced antinucleons from three different simulation models. The solid line shows data from HIJING, the dashed line from NEXUS and the dotted line from VNI.*

1.4 Net Nucleon Spectra

Because of the conservation of baryon number, the final state of a nuclear collision contains more baryons than antibaryons. This excess of baryons

$$\#net\ baryons = \#baryons - \#antibaryons \tag{1.3}$$

corresponds to the number of nucleons from the incident nuclei which participate in the interaction. Therefore, the phase-space distribution of this baryon excess can be used to study the structure of the collision.

In a scenario in which the nuclei are mostly intransparent to each other, the baryons will be stopped and then reaccelerated by the energy stored in the collision region, losing most of the information about the initial state (Landau picture). In this case, the rapidity distribution of the net baryons will be peaked at mid-rapidity, similar to the distributions of the produced particles, a phenomenon observed in nuclear collisions around 1 GeV per nucleon.

In a scenario where the nuclei are more transparent, the baryons will only lose a small part of their kinetic energy. The remnants of the two nuclei will fly apart rapidly, retaining much of the information about their initial state and creating a meson-rich area with few net baryons in the middle (Bjorken picture). In this case, the net baryon distribution will

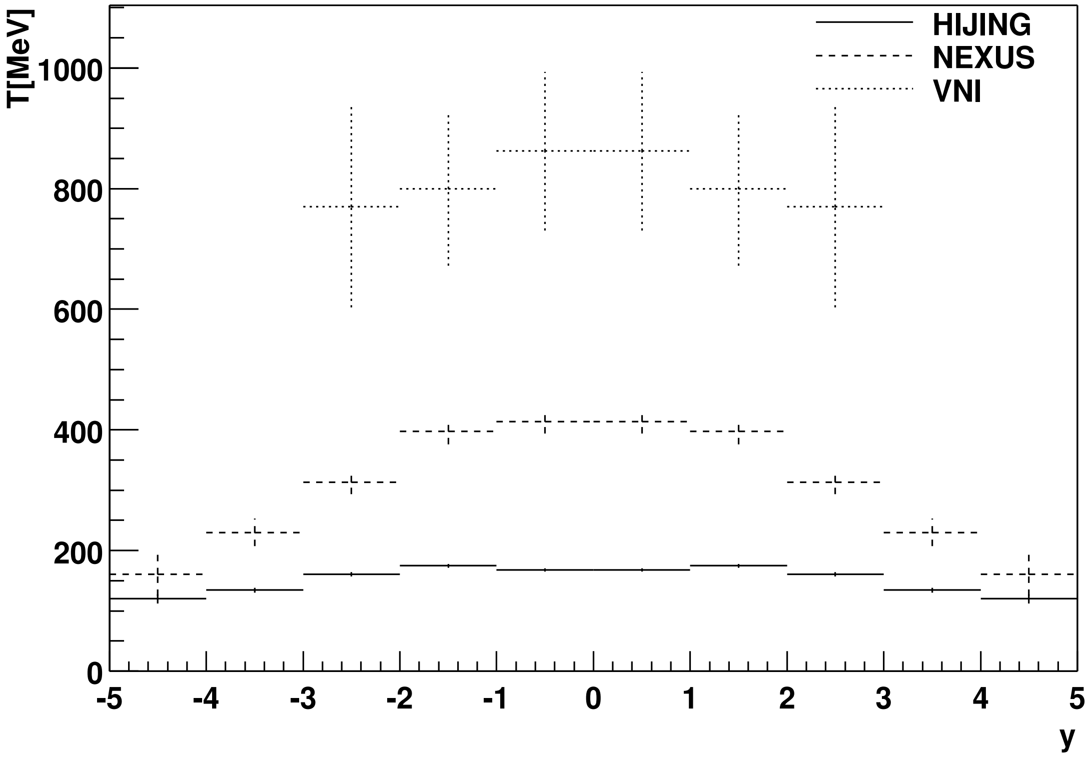

Figure 1.6: *Temperature parameters as functions of rapidity of antinucleons from three different simulation models. The solid line shows data from HIJING, the dashed line from NEXUS and the dotted line from VNI. The error bars show only the statistical error from the temperature fit.*

show two maxima close to the rapidity of the incident nuclei and very few net baryons around midrapidity.

None of the net nucleon spectra of the models in the comparison shows complete stopping of the net nucleons at midrapidity (see figure 1.7). Not very surprising, VNI, the parton cascade, shows the most stopping, whereas the pure string model HIJING is close to the picture of transparent nuclei with a baryon-free zone in the middle.

Remarkably, the integral over the net nucleon distribution in VNI is quite obviously smaller than in the two other models and also smaller than the number of nucleons in the initial state (394), which should be conserved in the collision (neglecting a very small number of heavier baryons decaying after leaving the detector). Although VNI does its calculation on the parton level and therefore does not conserve baryon number explicitly in the cascade, the difference between quarks and antiquarks should be kept constant, implying baryon conservation. One possible factor contributing to the lack of nucleons in the final state in VNI is that it is the only one of the three models that includes the formation of deuterons and other light nuclei, which were not counted in the present analysis. Furthermore, the sharp cutoff in all VNI spectra at $\mid y \mid= 4.5$ indicates that spectators (nuclei which do not take part in the interaction because of the finite impact parameter) are not included in the model output and, therefore, in this analysis.

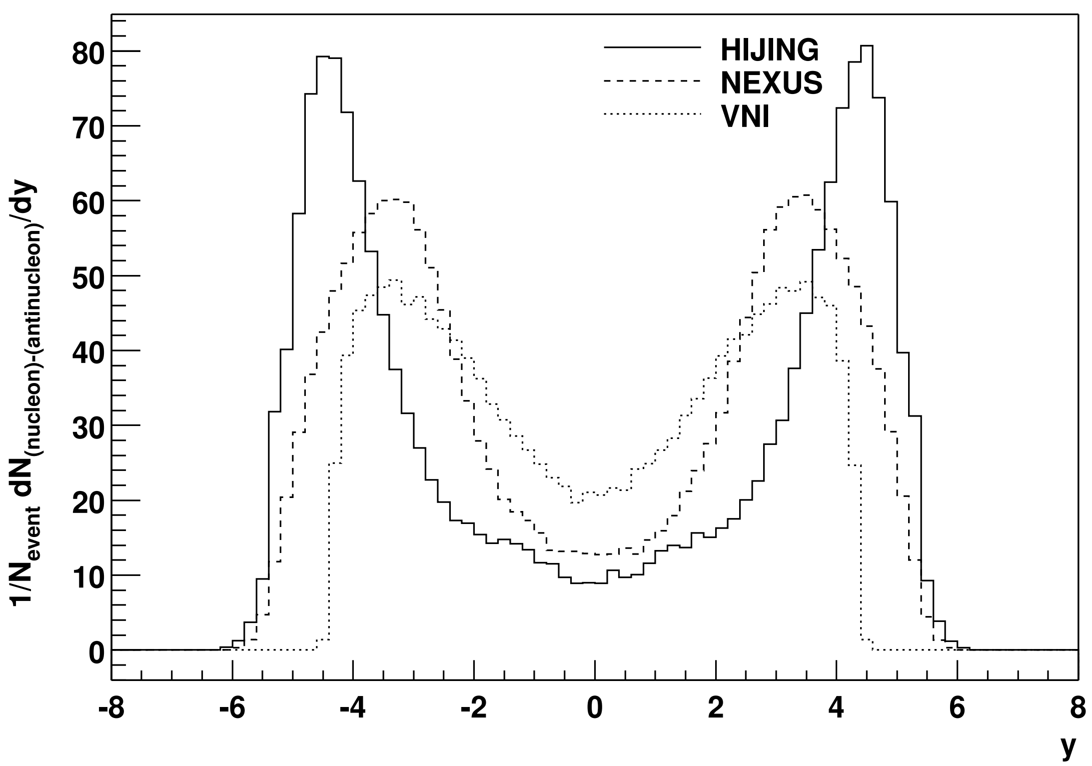

Figure 1.7: *Rapidity distribution of net nucleons (excess of nucleons over antinucleons, corresponding to the remainder of nuclons from the colliding nuclei) from three different simulation models. The solid line shows data from HIJING, the dashed line from NEXUS and the dotted line from VNI.*

Comparing the temperature parameters of the net nucleons (figure 1.8) to those of the produced antinucleons (figure 1.6) can test the hypothesis of mass-dependent temperature parameters by radial flow. In the case of radial flow, all nucleons and antinucleons, having the same mass, should show the same temperature parameters. If the net nucleons retain information on the initial state, however, their transverse momenta and temperatures may be smaller than those of the antinucleons, which were all produced in the collision. In the models studied, no such effect was observed. The data from NEXUS, which should not have radial flow, is consistent with a flow picture, at least for the nucleons and antinucleons. The net nucleons from VNI, on the other hand, show an unexpected temperature minimum at midrapidity, but the deviations from the antinucleon data in figure 1.6 are within the size of the error bars.

1.5 Net Positive Charge Spectra

In a detector without particle identification, the baryon and antibaryon spectra discussed in sections 1.3 and 1.4 can not be measured directly. The net baryon measurement is further complicated by the fact that in the final state, a significant part of the baryons are neutrons, which are experimentally extremely difficult to discern from antineutrons,

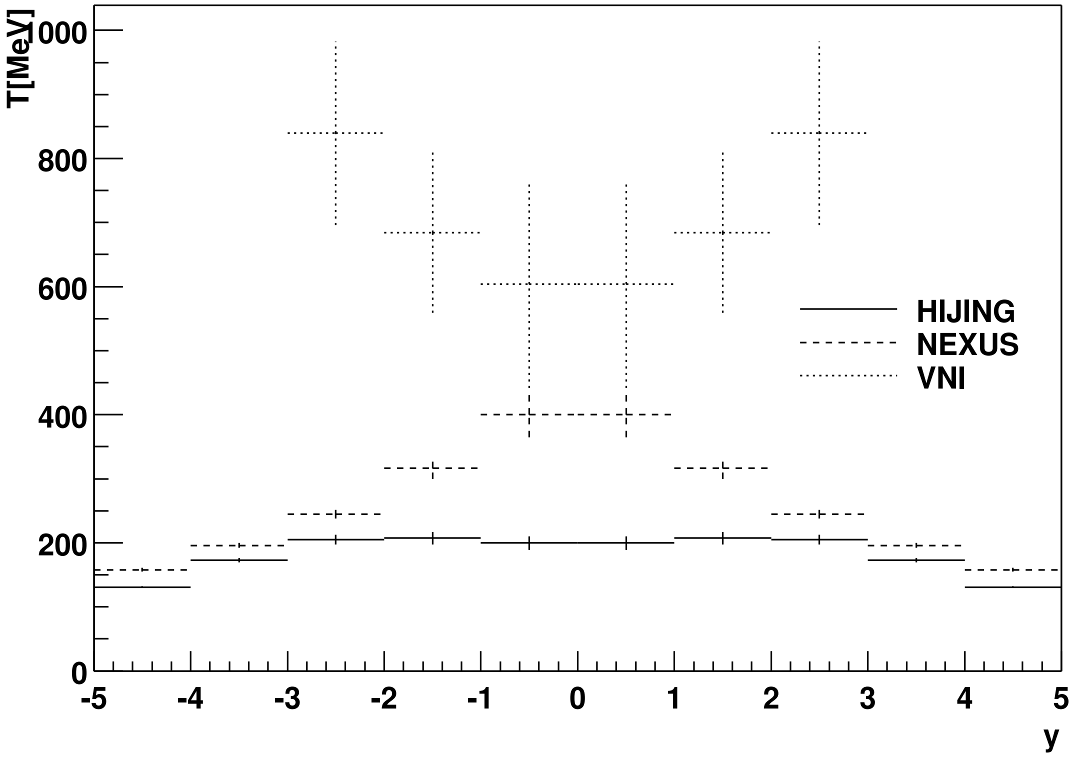

Figure 1.8: *Temperature parameters as functions of rapidity of net nucleons (number of nucleons minus number of antinucleons) from three different simulation models. The solid line shows data from HIJING, the dashed line from NEXUS and the dotted line from VNI. The error bars show only the statistical error from the temperature fit.*

if they can be measured at all. Only the weak lambda decays allow the separation of baryons from antibaryons purely from charge and momentum measurements, but lambda decay reconstruction is only possible with large errors and covers only a small part of all produced baryons and antibaryons.

However, even if protons can not be separated from charged mesons and no lambda reconstruction is possible, the remnants of the incident nuclei can be studied from the charge spectra. Because the incident nuclei contain protons and charge is also a conserved quantum number, there is an excess of positive over negative charges in the final state of a nuclear collision. This excess of positive charges can be used to measure the transparency of the nuclei in a similar way as the baryon excess. However, it is not obvious that the results will be identical, as the transport mechanisms for charge and baryon number may be different.

It should also be noted that at high collision energies, the excess of positive over negative charges is a small difference of large numbers and therefore extremely sensitive to measurement biases.

Figure 1.9 shows that the rapidity distribution of the net positive charges resembles that of the net baryon number (figure 1.7), scaled down by the ratio of charge divided by mass of the incident nuclei. For all event generators, the distributions have similar shapes and

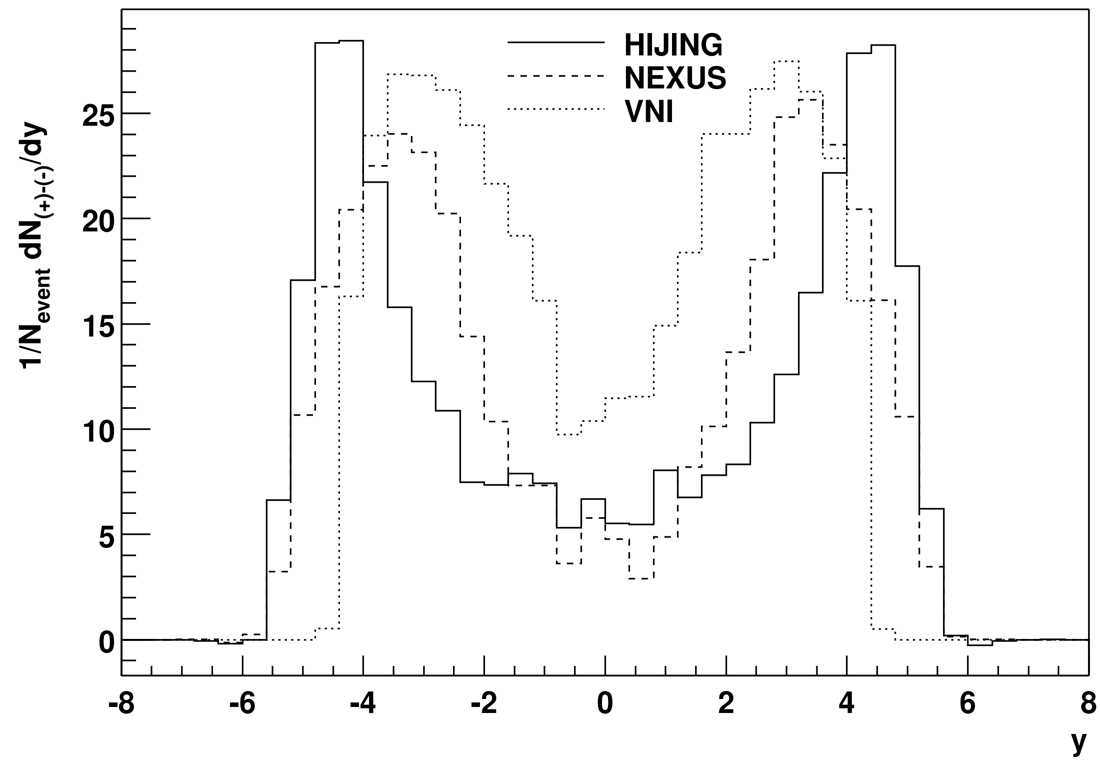

Figure 1.9: *Rapidity distribution of net positive charges (excess of positively charged over negatively charged particles, corresponding to the initial proton charge from the colliding nuclei) from three different simulation models. The solid line shows data from HIJING, the dashed line from NEXUS and the dotted line from VNI.*

are peaked at the same rapidity as the net baryon distributions. Merely the ratios of maximum to minimum values indicate that the stopping may be slightly overestimated when charge is used as a measure of baryon number.

This comparison, however, does not determine whether the observed excess of positive charges actually results from an excess of positive baryons (which could only be protons) in the final state, or if the charge has been transferred to other particles. In the first case, also the temperature parameters of the net positive charges should be similar to those of the net baryons. As a comparison of figure 1.10 with figure 1.8 shows, this is the case to a certain degree with respect to the shapes of the y-dependencies, but shifted to lower temperatures in VNI and NEXUS and to higher ones in HIJING.

Calculating transverse mass spectra of net positive charges suffers from the systematic problem that to calculate the transverse mass without particle identification, a rest mass has to be assumed. This mass assumption will have a significant impact on the reconstructed temperatures and the quality of the fit. The most probable rest mass for an unidentified particle is the pion mass, but if the net positive charge signal can be linked to protons, the spectra should better be fitted with the proton mass. This indicates that without other information about the distribution of baryon number it is problematic to use transverse spectra of net positive charge to measure baryon temperatures.

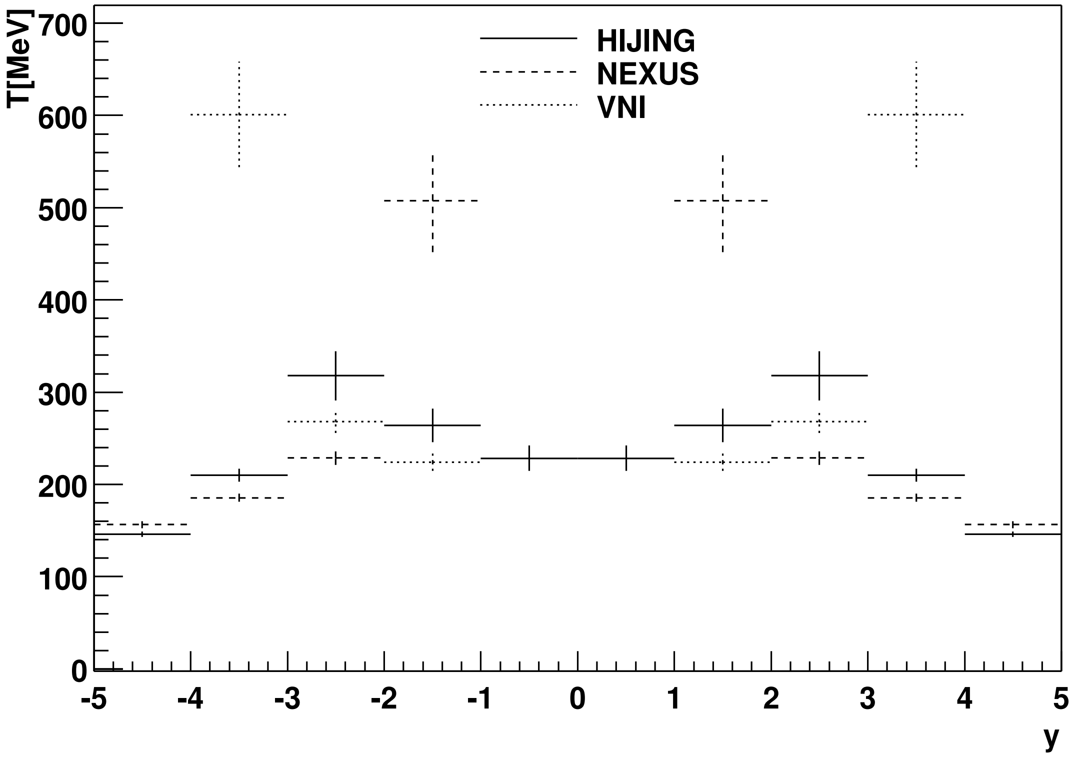

Figure 1.10: *Temperature parameters, calculated assuming the proton mass, as functions of rapidity of net positive charges (number of positive minus number of negative charges) from three different simulation models. The solid line shows data from HIJING, the dashed line from NEXUS and the dotted line from VNI. The error bars show only the statistical error from the temperature fit.*

To better understand the combination of particles contributing to the excess of positive charges, net charge rapidity distributions were analyzed for different particle species separately. The rapidity distribution of the proton excess over antiprotons in figure 1.11 and a comparison with figure 1.9 indicate that a significant part of the net positive charges are actually stored in the protons. Only in VNI, a significant part of the net positive charge spectra obviously does not result from protons, whereas in HIJING, the excess of protons over antiprotons is even larger than that of positive over negative charges.

A further potential carrier of the positive charge excess are the kaons, shown in figure 1.12. In VNI, the kaons carry almost as much positive charge as the protons and even dominate at midrapidity. In the string models, their contribution is smaller. Remarkably, the shapes of the net positive kaon spectra from the three models look completely different.

In principle, the net positive charge could also be included in the pions. As seen in figure 1.13, this is not observed, and there is even a small excess of negative over positive pions at least in the string models.

A simple explanation for this result is that in the final state, all baryons must have decayed either to protons or to neutrons. For each net baryon in the final state, there is a certain probability for it to be positive, whereas it can not be negative, so an excess

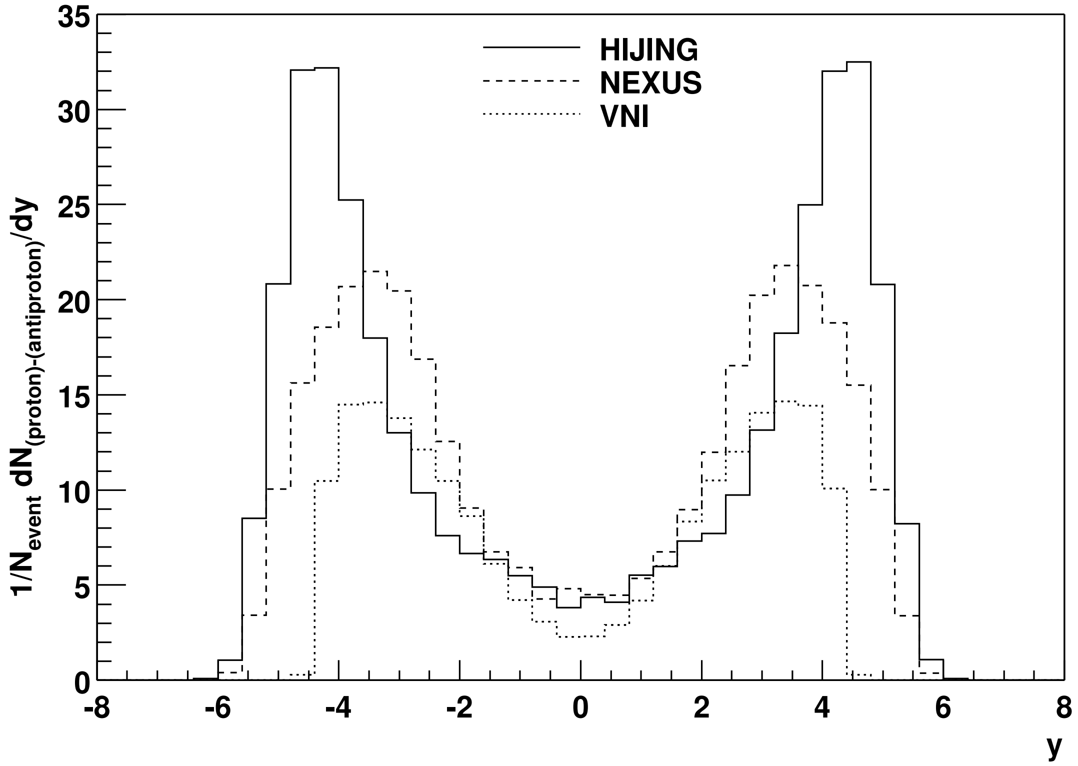

Figure 1.11: *Rapidity distribution of net protons (excess of protons over antiprotons) from three different simulation models. The solid line shows data from HIJING, the dashed line from NEXUS and the dotted line from VNI.*

of baryons over antibaryons will automatically lead to an excess of positive over negative charges.

In a hadronic scenario, there can of course be intermediate baryonic states of negative charge, like the N and Δ resonances or the Σ^-, the Ξ^- and the Ω^-. When they decay, ultimately to neutrons or protons, their negative charge will most probably be deposited in π^-.

It can be concluded that even without particle identification, the FTPCs will be able to provide significant information on stopping through the study of net charge distributions.

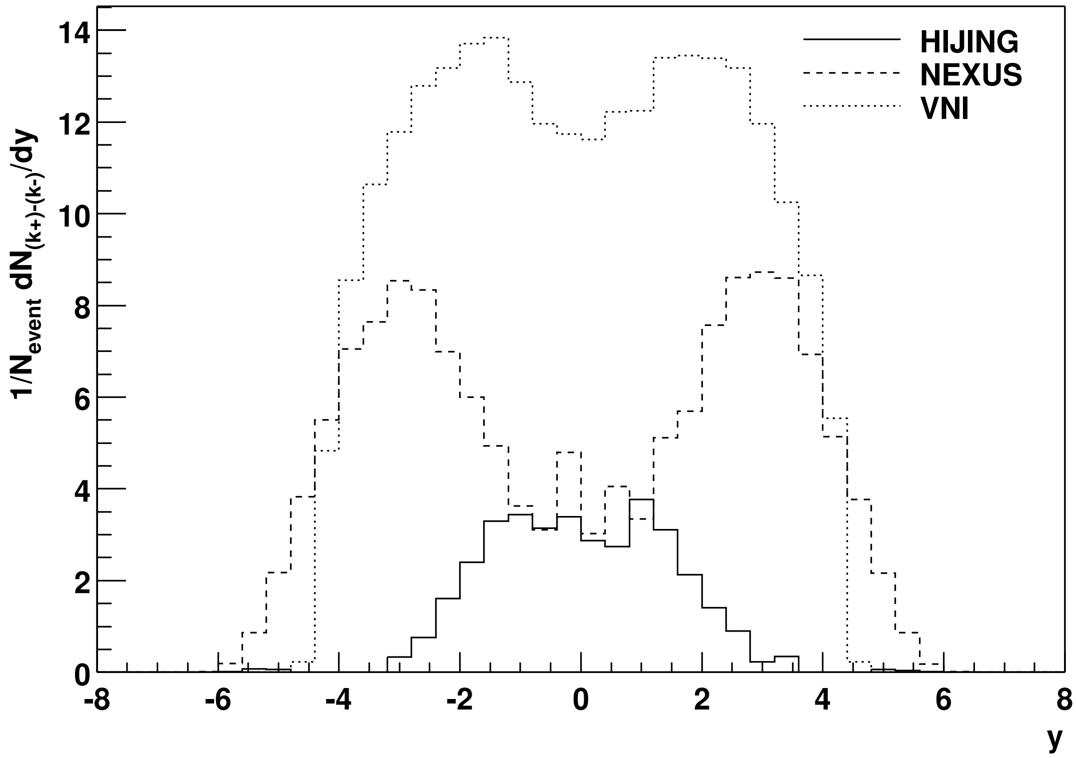

Figure 1.12: *Rapidity distribution of net positive kaons (excess of positive over negative kaons) from three different simulation models. The solid line shows data from HIJING, the dashed line from NEXUS and the dotted line from VNI.*

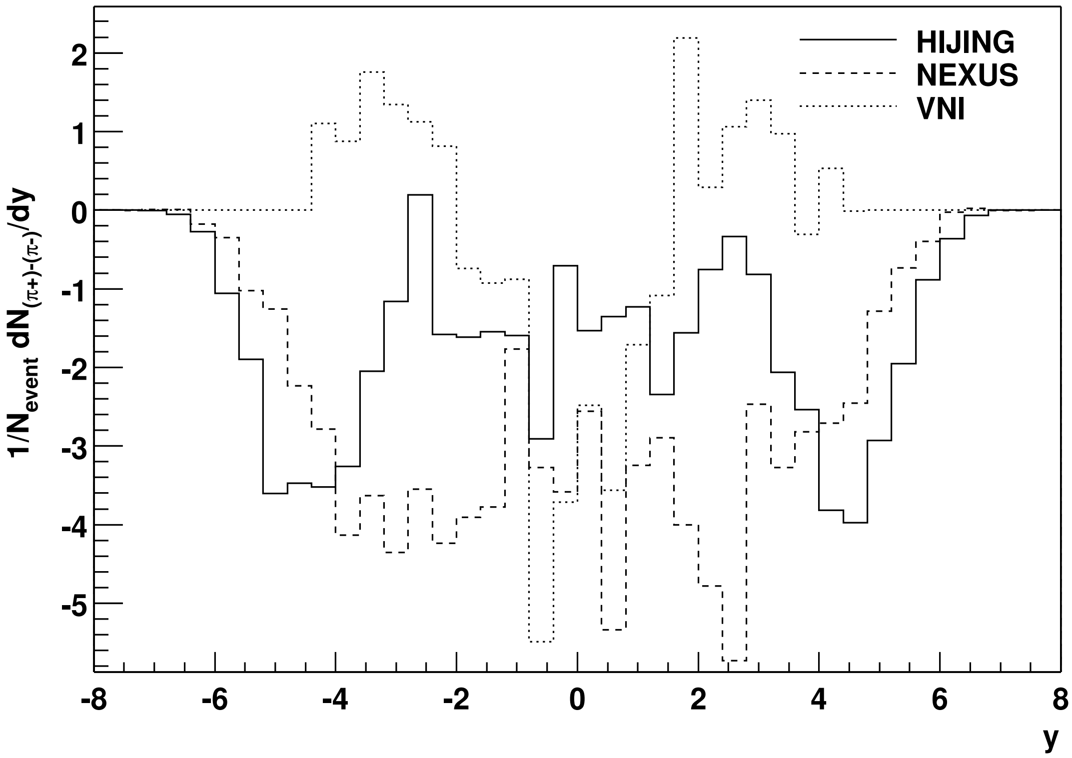

Figure 1.13: *Rapidity distribution of net positive pions (excess of positive over negative pions) from three different simulation models. The solid line shows data from HIJING, the dashed line from NEXUS and the dotted line from VNI. The fluctuations arise because each entry is the difference of two very large numbers.*

Chapter 2

Event-by-Event Analysis in the FTPCs

Discussions on the possibilities offered by the FTPCs in the measurement of particle spectra integrated over large numbers of events can be found in [Kon97] and [Bie98]. Therefore, the present chapter will focus on the reconstruction of properties of single events. This, of course, limits the study to observables that can be reconstructed with sufficient accuracy in every single event (unlike, for example, the number of strange particle decays).

To compare the detector response to different physics scenarios, the data used was taken from the three event generator packages studied in chapter 1. The available data included between 1500 and 2000 events for each package. All distributions of event properties in the following sections correspond to 1500 events for each event generator.

2.1 Determining the Correction Factors

Because of the relatively low reconstruction efficiency over large parts of the acceptance, the corrections which are necessary to derive the experimental spectra from the reconstructed tracks are relatively large. As these corrections determine the size of the systematic errors in the results, their reliability is vital to the quality of the final data, especially when the magnitude of the corrections is large. In the FTPC, this is further complicated by the non-negligible contamination of the reconstructed track sample with unwanted tracks and by the limited momentum resolution.

If the efficiency and contamination are known with sufficient precision, they can in principle be used for the correction directly, by subtracting the contamination from the reconstructed tracks and scaling the result with the inverse reconstruction efficiency. This approach, however, has two important drawbacks:

- The contamination can only be determined for fully simulated events, and only in simulations where the reconstructed tracks can be directly matched to the simulation input. This complicates the use of very detailed simulations at the electronics level and makes it impossible to use measured data as background. Therefore, the

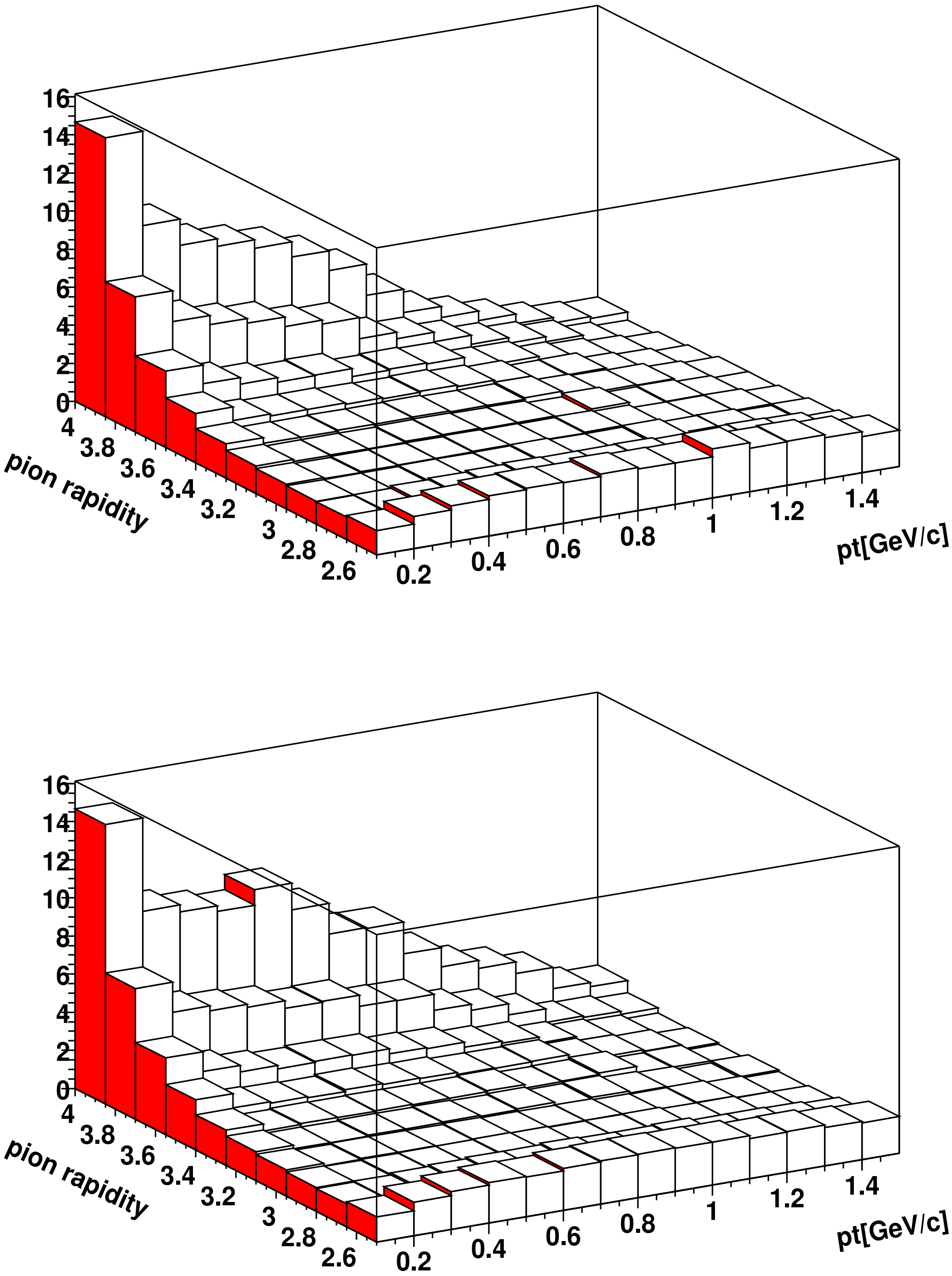

Figure 2.1: *Correction factors for reconstruction losses for negative (top) and positive (bottom) particles reconstructed in the FTPCs. In the analysis of particle spectra, for each interval in transverse momentum and rapidity (assuming pion mass), the number of entries is multiplied by the corresponding correction factor. The figure shows the correction factors for data produced by the NEXUS event generator.*

calculation of both the reconstruction efficiency and the contamination suffer from the problem that the simulation input will never completely agree with the physics in the real collision and that the detector response simulation can never include all the details that might affect the detector's performance.

- The effects of the momentum resolution have to be taken into account separately. A finite momentum resolution will generally shift more track momenta from densely populated regions of phase-space to less densely populated regions than vice-versa. Although it is in principle possible to correct for this effect, this task is complicated by the fact that the momentum resolution itself varies across the phase-space covered by the detector.

Therefore, for this analysis, a much simpler correction method was used. For a large set of simulated events, in each segment of phase-space, the number of simulated tracks within the geometric acceptance of the FTPC was divided by the number of tracks reconstructed in the same segment of phase-space. The resulting correction factors can directly be multiplied with the number of measured tracks in the corresponding segment of phase-space to account for efficiency and contamination as well as for the effects of momentum resolution. Moreover, this procedure permits the use of the more realistic slow simulation chain.

For real data, correction factors can also be determined by embedding simulated tracks in the data of a measured event and analyzing the reconstructed tracks added by this embedding procedure. However, correction factors determined from embedding alone may give an overly optimistic view of the contamination. Furthermore, the number of tracks embedded should be small compared to the number of tracks in the event; otherwise the embedded tracks will affect each other instead of just being affected by the background event. Therefore, it may be advisable to at least compare the correction factors derived from embedding to those derived from a full simulation which has similar track densities as the observed event.

To determine the correction factors, the phase-space should be segmented in the same intervals used in the subsequent physics analysis. Therefore, the correction factors were calculated for intervals in transverse momentum and rapidity (instead of the pseusorapidity used in the calculation of efficiecy and contamination), with the rapidity being calculated assuming the pion mass.

Figure 2.1 shows the correction factors for negative and positive charges in the geometrical acceptance of the FTPC, calculated with the described procedure using the slow simulation chain on events from the NEXUS event generator. Separate correction tables for both charges are necessary because the blind areas at the sector boundary extrapolate inward in radius along the drift of the negatively charged electrons. Therefore, the probability of reconstructing a track from a negative particle close to a sector boundary is slightly larger than for a positive particle. This effect could be eliminated by introducing azimuthal cuts in the geometrical acceptance. For very forward rapidities and small transverse momenta, the correction factors are large, because few particles in this rapidity region leave a track in the FTPC that is long enough to be reconstructed. Therefore, it may be useful to eliminate this region of phase-space from an analysis to minimize the errors.

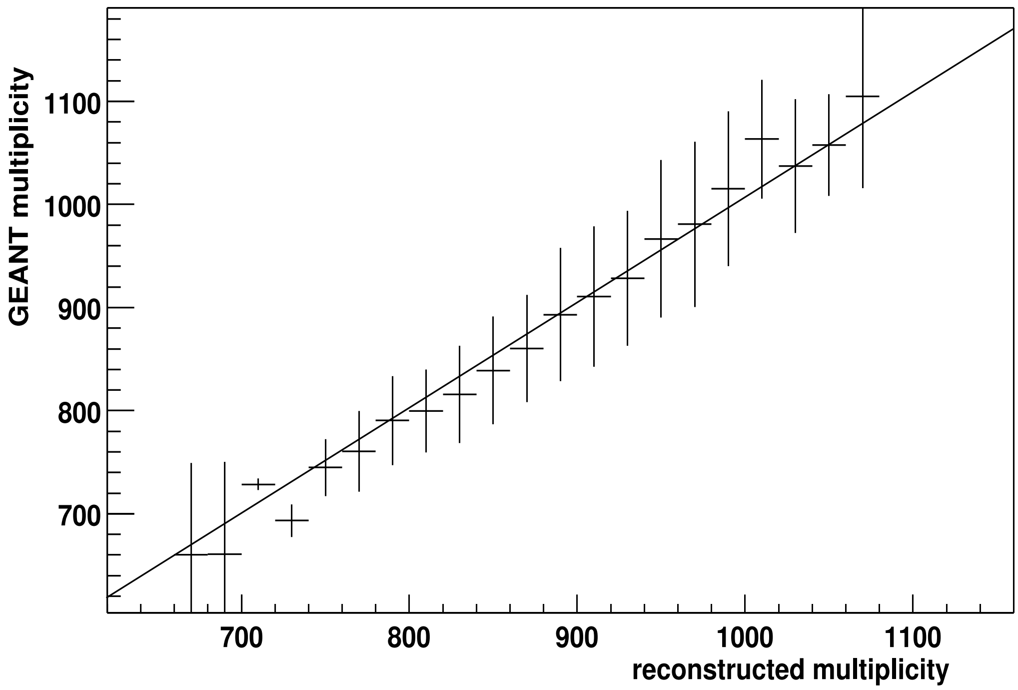

Figure 2.2: *Reconstruction capability for charged particle multiplicity in the acceptance of the FTPCs. The figure shows the event multiplicity simulated with GEANT versus the value reconstructed in the FTPC analysis chain. Error bars correspond to the width of the distribution of input values for the respective reconstructed value. The analysis is based upon the reconstruction of approximately 2000 events from the NEXUS event generator. A diagonal line is included to guide the eye.*

2.2 Reconstruction of Multiplicity Fluctuations

The simplest event property to analyze in a tracking detector is the charged particle multiplicity within the detector's acceptance. In the FTPC, including only particles originating from the main interaction point, the acceptance is almost identical to a fixed range in pseudorapidity. To account for the low efficiency and high contamination of this track sample at small transverse momenta, particles with a transverse momentum of less than 100 MeV/c were excluded from the analysis.

The contribution from protons and antiprotons as well as from charged leptons is small compared to the charged meson production in this rapidity range. Therefore, the charged particle multiplicity is dominated by the meson production in the collision, which again consists mostly of pions. Figures 1.1 indicates that differences in the mean values of the pion multiplicity in the FTPC between the three event generators are not expected to be large. Differences in the mean values of the charged particle multiplicities will mostly result from the different kaon multiplicities, seen in figure 1.3.

However, the variations of the charged multiplicity from event to event may yield more information. First, it is interesting to find out whether the widths of the multiplicity distributions allow to distinguish between different scenarios at all. Second, the presence

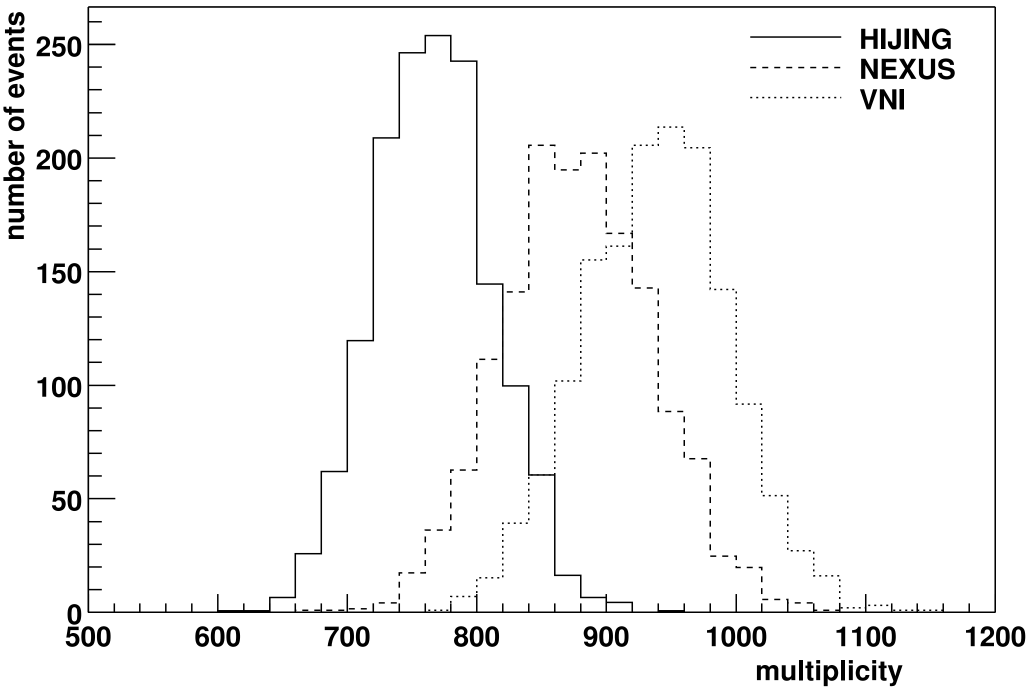

Figure 2.3: *Distributions of the reconstructed charged particle multiplicity in the FTPCs for three different event generators. The solid line shows events from the HIJING event generator, the dashed line from NEXUS and the dotted line from VNI.*

of a phase transition may lead to dynamical fluctuations, which may range from a widening of the multiplicity distribution a distribution showing to two distinct event classes with and without the phase transition.

Because of the limited reconstruction efficiency and non-zero contamination, the number of tracks reconstructed in the FTPC will generally not be identical to the actual charged particle multiplicity in the FTPC acceptance. Ideally, the correction factors presented in section 2.1 should correct for this effect, with the exception of statistical errors. However, both tracking efficiency and contamination can depend on the track density and, therefore, on the charged particle multiplicity. In this case, the linear correction factors would not allow to derive the charged particle multiplicity from the number of reconstructed tracks. To test this, the known charged particle multiplicity within the geometrical acceptance of the FTPC from simulations was compared to the multiplicity reconstructed in the FTPC (after the application of correction factors). The resulting figure 2.2 shows within which range of values the actual track multiplicity fluctuates for each reconstructed multiplicity value. The figure indicates that, in spite of significant fluctuations of the single values, the multiplicity is on average reconstructed correctly, even in the case of very high or very low multiplicities. Global effects of track density, which would lead to a nonlinear dependence, are not observed.

Figure 2.3 shows the distributions of the reconstructed charged particle multiplicity in the acceptance of the FTPC from the three event generators. The multiplicity distributions differ significantly in their mean values, but all three have similar shapes, which are in good agreement with Gaussian functions. Fitting Gaussian curves to the distributions

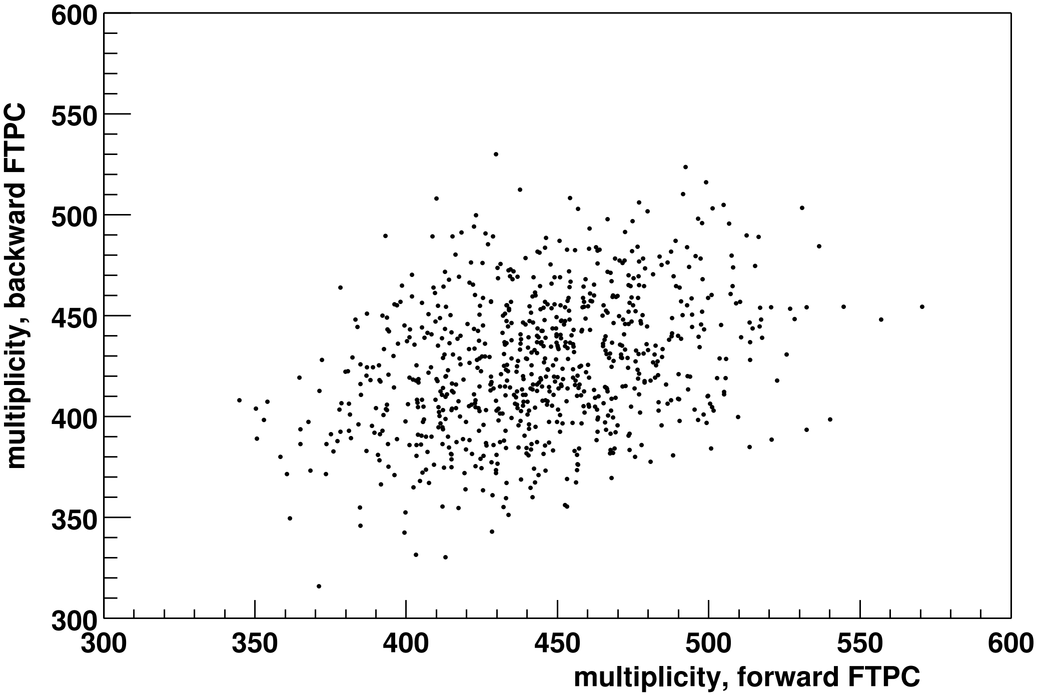

Figure 2.4: *Correlation of charged particle multiplicities in the two FTPCs. The figure shows the multiplicity in the backward (East) FTPC versus the multiplicity in the same event in the forward (West) FTPC in events simulated with the NEXUS event generator.*

yields a mean value of 766.9 with a sigma of 44.4 for HIJING, a mean value of 878.2 with a sigma of 56.9 for NEXUS and a mean value of 938.2 with a sigma of 55.1 for VNI. The widths of the distributions can be fully explained by statistical fluctuations, variations of the impact parameter, acceptance shifts from the fluctuation of the collision point in the interaction region of the beams and the fluctuations introduced by the reconstruction, which can be estimated from figure 2.2. Dynamical fluctuations are not present at a scale that could be observed in this analysis.

Transferring this analysis to actual experimental conditions shows a problem of event selection. Whereas in the simulation, the event generators simulated collisions with impact parameters between the colliding nuclei ranging up to 3 fm, the impact parameter can not be directly measured in the experiment. The selection of events with small impact parameter can be done independently from the measured particle production if the energy of the spectators (nucleons not affected by the collision) can be measured. As this is extremely difficult in a collider geometry, the STAR trigger system estimates the impact parameter by measuring the charged particle multiplicity in a pseudorapidity range of $\eta < 2$. If dynamical fluctuations affect the event as a whole, this event selection may introduce a bias in multiplicity fluctuations measured in other regions of phase-space.

An interesting way of studying multiplicity correlations between different regions of phase-space is to compare the charged particle multiplicities measured in the two FTPCs. In this case, possible efficiency problems should compensate each other, because both FTPCs are identical in construction and symmetrical in position. However, the acceptance shift

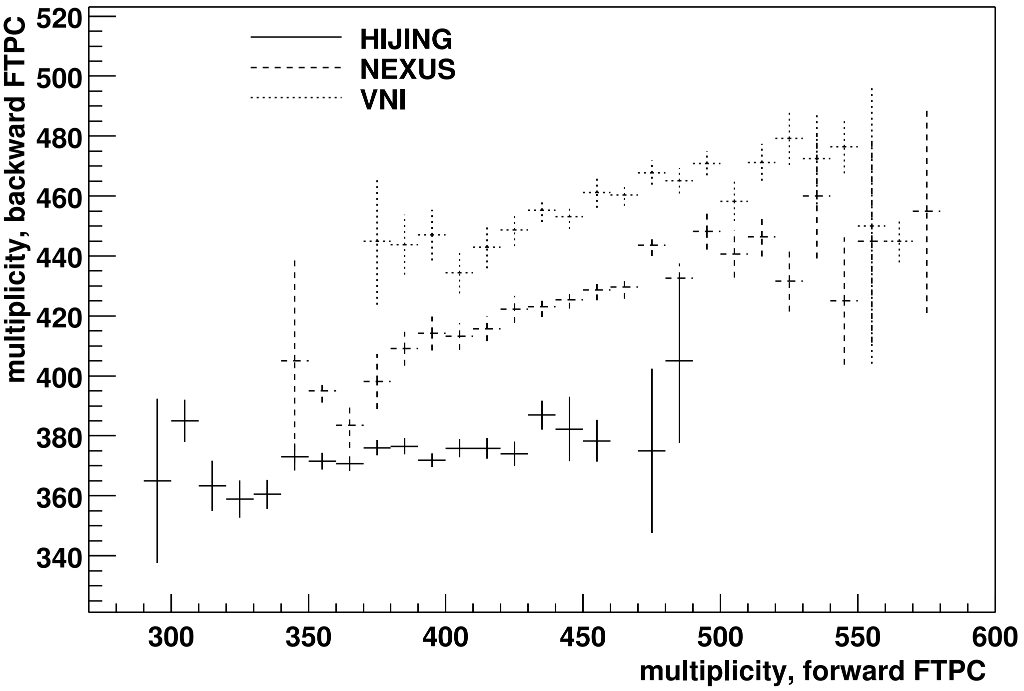

Figure 2.5: *Correlation profile of charged particle multiplicities in the two FTPCs. The figure shows the multiplicity mean and error in the backward (East) FTPC versus the multiplicity in the same event in the forward (West) FTPC for the three tested event generators (HIJING = solid line, NEXUS = dashed line, VNI = dotted line).*

of the two FTPCs when the interaction point shifts in z introduces an anticorrelation between the multiplicities measured in the two chambers. To eliminate this effect, for this study, only events with a main interaction point close to the center of the STAR detector were accepted.

In figure 2.4, the distribution of charged particle multiplicities in the two FTPC is plotted for events from the NEXUS event generator. The correlation is clearly visible. Calculating the correlation coefficient according to Pearson

$$r = \frac{\sigma_{xy}}{\sigma_x \sigma_y} \tag{2.1}$$

returns a value of $r = 0.33$. In HIJING ($r = 0.12$) and VNI ($r = 0.23$), the correlation is less pronounced. A different way of visualizing the correlation is to plot the mean values (averaged over events) of the multiplicity in one detector as a function of the multiplicity in the other detector (see figure 2.5). The correlation is visible in NEXUS and VNI, but not in HIJING.

These results indicate that the multiplicity fluctuations are at least in part caused by fluctuations of a property of the whole event. Besides dynamical fluctuations in the event generator, a possible candidate for this property is the impact parameter, which determines the number of nucleons participating in the interaction and, thus, the number of initial nucleon collisions. Naively, one would expect a model without any reinteractions to yield multiplicities that are linear in the number of initial collisions, whereas in a model with rescattering, a densely populated phase space would lead to additional collisions and additional particle production. On the other hand, this effect should not be as pronounced as it appears in this data, as the total multiplicities differ only on the order of 20%, and the authors of all three models claim to also describe proton-proton collisions correctly. If all models yield the same multiplicity for two participating nucleons and differ by about 20% for almost 400 participating nucleons, the small variation resulting from the finite impact parameters should not be that significant.

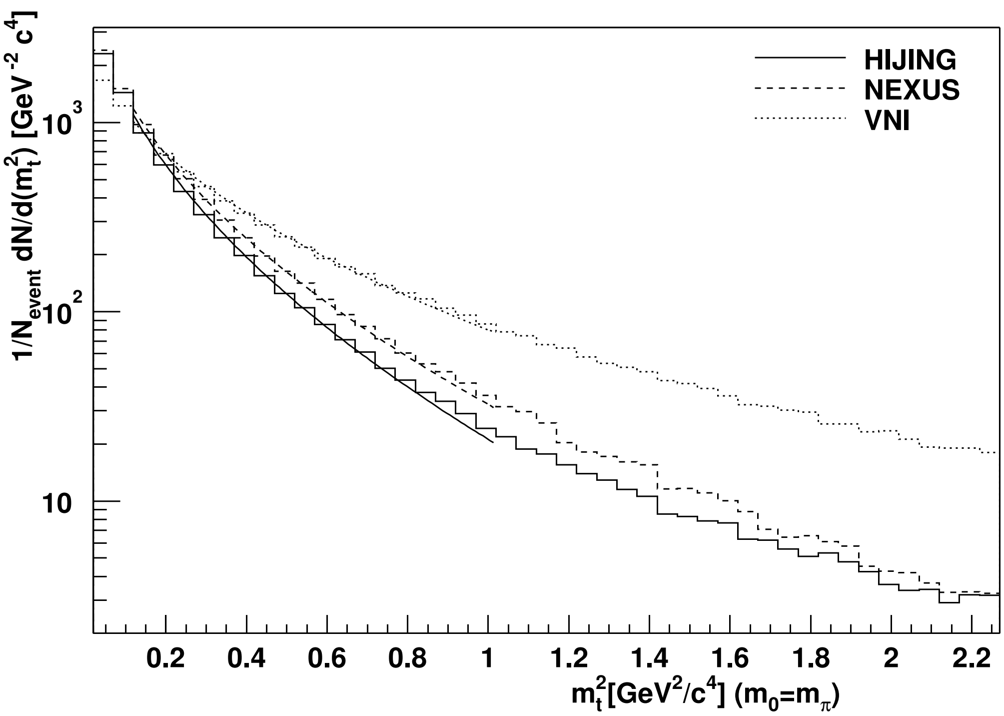

Figure 2.6: *Reconstructed distributions of the square of the transverse mass of negatively charged particles in the FTPCs averaged over large event samples for three different event generators. The solid line shows data from the HIJING event generator, the dashed line from NEXUS and the dotted line from VNI. The curved lines are exponential fits in the transverse mass corresponding to temperatures of 166 MeV for HIJING, 181 MeV for NEXUS and 258 MeV for VNI.*

2.3 Reconstruction of Transverse Momentum Fluctuations

Given the different model predictions for the rapidity dependence of the temperature parameters (figures 1.2, 1.4, 1.6, 1.8 and 1.10), the measurements of transverse momentum spectra in the FTPCs can have special relevance when seen together with the results from the TPC. As there is no particle identification available in the FTPC, pion spectra can only be approximated with negative particle spectra. The track sample from negatively

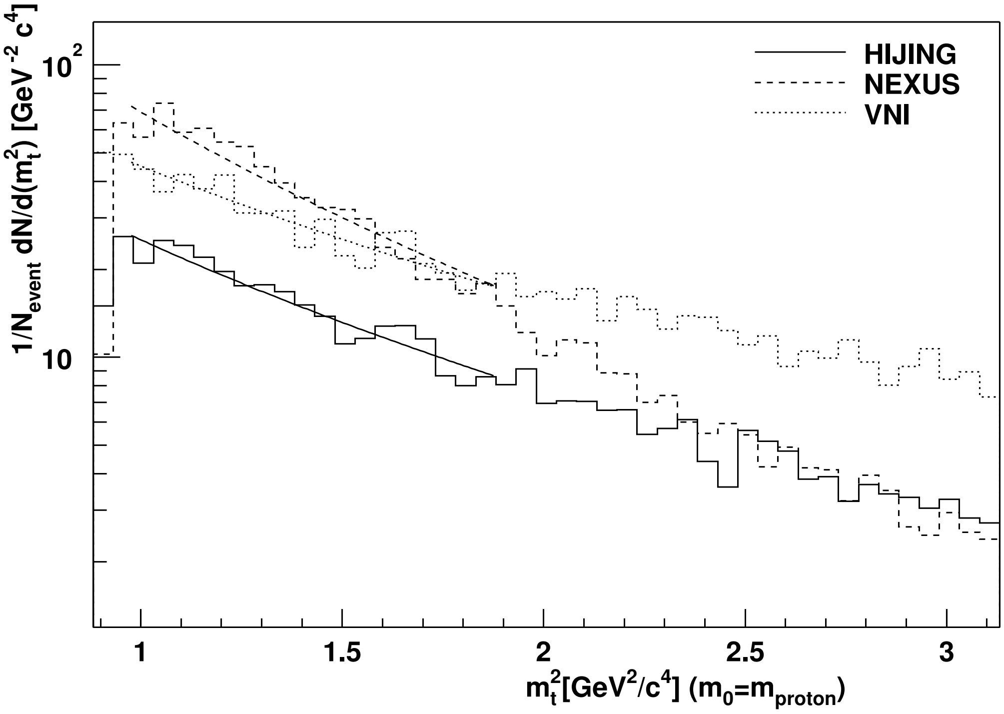

Figure 2.7: *Reconstructed distributions of the square of the transverse mass of net positive particles (excess of positive over negative charges) in the FTPCs averaged over large event samples and calculated under the assumption of the proton mass for three different event generators. The solid line shows data from the HIJING event generator, the dashed line from NEXUS and the dotted line from VNI. The curved lines are exponential fits in the transverse mass corresponding to temperatures of 335 MeV for HIJING, 270 MeV for NEXUS and 389 MeV for VNI.*

charged particles does not contain any baryons but only the smaller antibaryon contamination and a smaller number of kaons because of the positive charge excess in the kaons shown in figure 1.12.

Spectra of transverse momentum of negatively charged particles, transformed into the square of the transverse mass and averaged over many events, can be seen in figure 2.6. In the fitted region, the spectra are all well described by exponential fits in the transverse mass (equation 1.2), with a small excess in the region of high transverse mass values, where hard scattering processes become more and more relevant.

The temperature parameters from the exponential fits show a remarkably good agreement with the temperature parameters of pions produced by the event generators in the rapidity region accessible to the FTPC, shown in figure 1.2. As this is the case for all three event generators, it can be assumed that the correction factors are sufficient to correct for the errors in tracking and momentum reconstruction, at least for the purpose of determining temperature parameters. Also, the kaon and antibaryon contaminations do not seem to have a significant impact on the negative particle temperature parameters.

The corresponding net positive particle spectra are shown in figure 2.7. Being calculated as the difference of two large numbers, they suffer from the obvious problem of large sta-

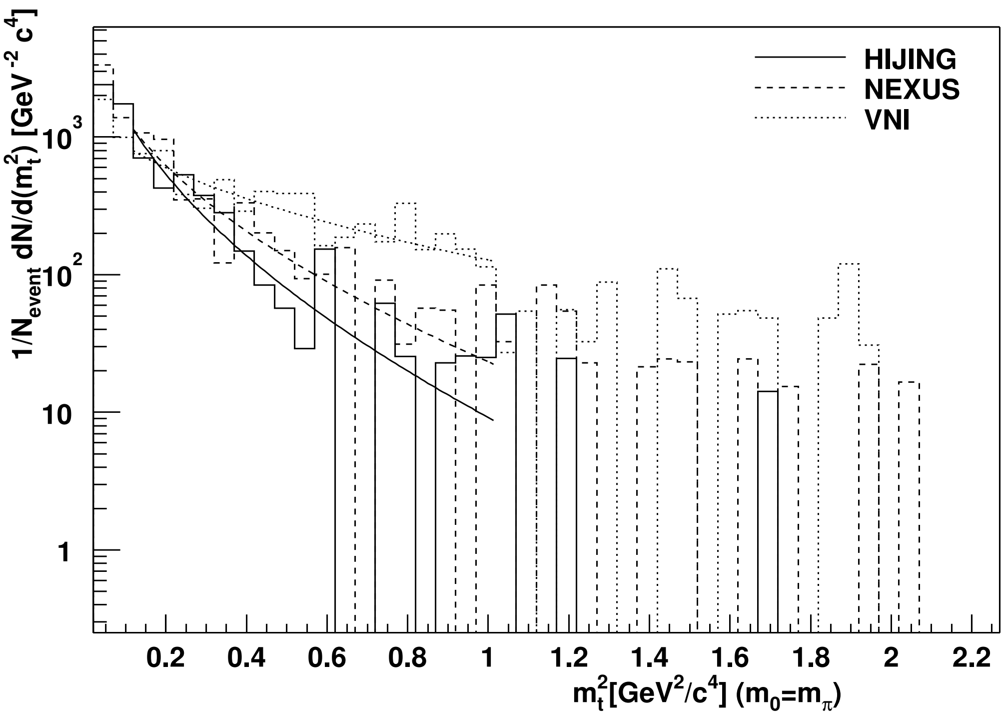

Figure 2.8: *Reconstructed distributions of the squared transverse mass and exponential fits of negatively charged particles in the FTPCs in a single event for three different event generators. The solid line shows events from the HIJING event generator, the dashed line from NEXUS and the dotted line from VNI.*

tistical fluctuations, which also reduce the quality of the temperature fits. Furthermore, it is obvious that at least the fit to the NEXUS data does not agree very well with the shape of the spectrum, especially in the region of small transverse masses, so the fitted temperature may be too high.

In addition, the net positive particle spectra suffer from a systematic problem: as the particle type and therefore the rest mass of the measured particles are unknown, the transverse mass has to be calculated using an assumption for the rest mass. This can be the proton mass if the net positive charge spectrum actually reflects the distribution of the protons reasonably well. However, in chapter 1 it was shown that the contribution from kaons is not negligible and even varies between the different model predictions. Without access to particle identification, there is no obvious, model-independent solution to this problem.

If the number of entries in the spectrum is large enough, it is also possible to calculate temperature parameters for single events. This condition is obviously not fulfilled for the excess of positive over negative charges. The negatively charged particle spectra for a single event (figure 2.8), however, have sufficiently large numbers of entries, and the temperature fits describe the shapes of the spectra reasonably well.

Figure 2.9 shows the reconstruction capability of the FTPCs for event-by-event temperature parameters in the simulated data. Simulated and reconstructed event temperatures agree reasonably well in a region between 120 MeV and 220 MeV reconstructed tempera-

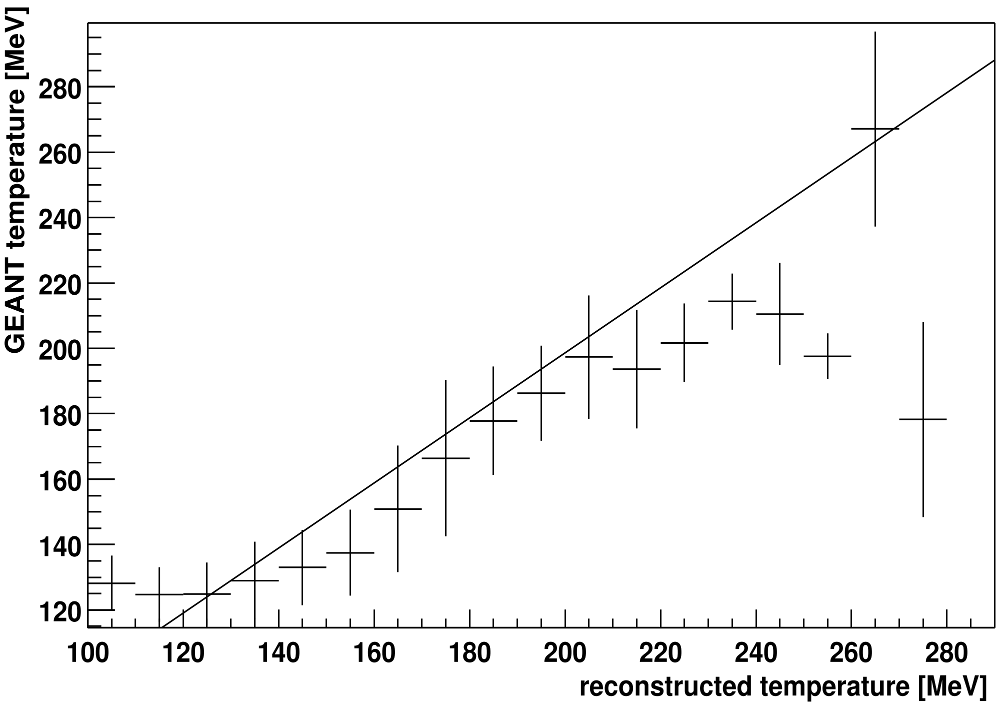

Figure 2.9: *Reconstruction capability for the temperature parameter describing the charged particle transverse momentum distribution in the acceptance of the FTPCs in single events. The figure shows the temperature parameter simulated with geant versus the value reconstructed in the FTPC analysis chain. Error bars correspond to the width of the distribution of input values for the respective reconstructed value. The figure is based upon the simulation of approximately 800 events from different event generators. A diagonal line is included to guide the eye.*

ture, whereas the more extreme reconstructed values are not appropriate representations of the input data. A possible reason is that this figure was generated using the correction factors derived from NEXUS, which were then applied to a mixed sample of events from different generators. In the range of temperatures covered by the NEXUS data, the reconstruction is correct. In the other figures, the data from each event generator was corrected with its appropriate correction factors. This shows that while the correction factors are not very sensitive to multiplicity, they are affected by the spectral shape of the data. Consequently, the correction factors applied to measured data should be derived from a simulation which reproduces the spectral shape of the measured data as well as possible, and they should be crosschecked using the embedding technique.

The distributions of reconstructed event-by-event temperature parameters (figure 2.10) show a significant overlap between the distributions from the different models. The temperature distributions have a mean value of 155.1 MeV with a standard deviation of 15.56 MeV for HIJING, a mean value of 169.2 MeV with a standard deviation of 16.9 MeV for NEXUS and a mean value of 233.2 MeV with a standard deviation of 26.6 MeV for VNI. This corresponds to a relative width of the distributions of slightly over 10% for all three event generators. The mean value of the event-by-event temperature parameters is in all three cases smaller than the temperature parameter of the average transverse mass

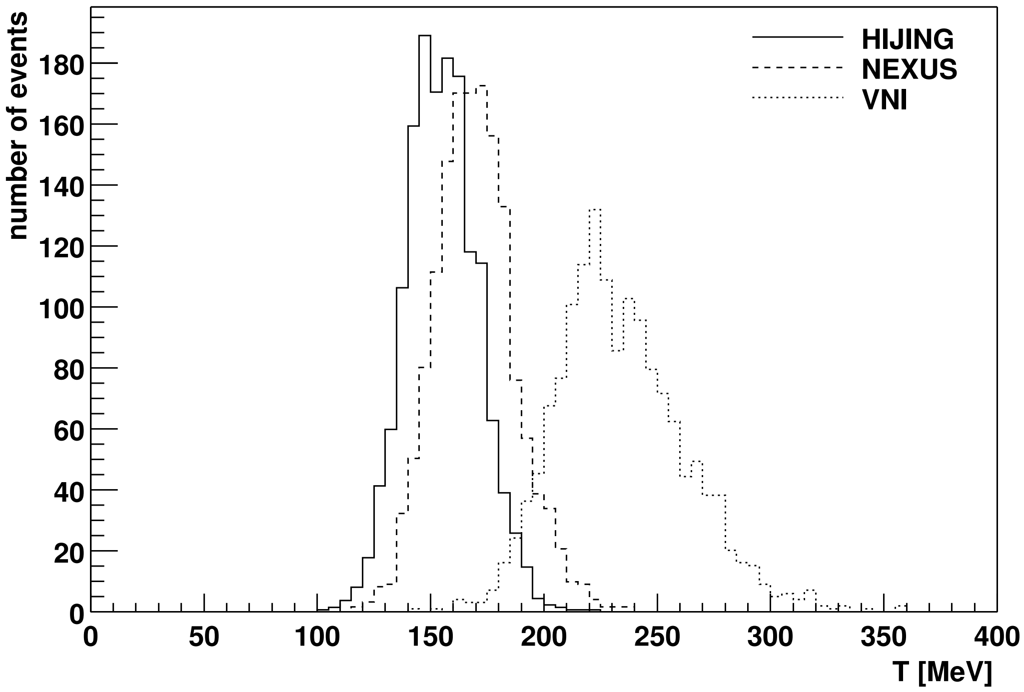

Figure 2.10: *Reconstructed distribution of temperature parameters per event in the FTPCs for three different event generators. The temperature parameters describe the transverse momentum distribution of negatively charged particles originating at the main interaction point. The solid line shows 1500 events from the HIJING event generator, the dashed line from NEXUS and the dotted line from VNI.*

distribution. This is understandable, as the temperature fits do not respond in a linear way to rare hard processes with high momentum transfer in a small number of events.

As event-by-event temperature parameters can be calculated individually for both FTPCs, the correlation between the two measured values can be studied. A strong correlation of the transverse momentum spectra in different regions of rapidity may indicate that a temperature exists as a global variable characterizing the collision as a whole. On the other hand, forward-backward correlations in the momentum distributions may also appear in string fragmentation mechanisms.

To give an impression on the magnitude of possible temperature correlations between the FTPCs, figure 2.11 shows the mean values of temperature parameters in one FTPC as functions of the temperature parameters in the other FTPC. By eye, correlations are not obvious. Calculating the correlation coefficient returns a value of 0.14 for NEXUS, 0.05 for VNI and -0.02 for HIJING. The temperature correlations are in all cases much weaker than the multiplicity correlations in figure 2.5, but in both observables, the correlation value is largest for NEXUS and smallest for HIJING. This may again result from the different models responding differently to small variations in the impact parameter.

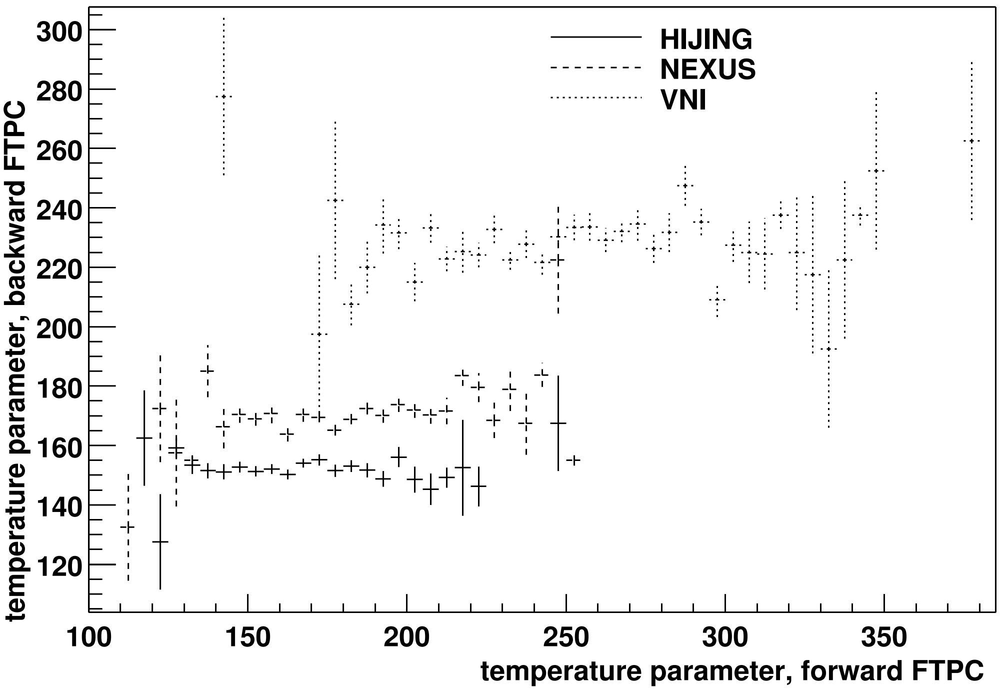

Figure 2.11: *Correlation profile of the charged particle temperature parameters in the two FTPCs. The figure shows the temperature parameter mean and error in the backward (East) FTPC versus the temperature parameter in the same event in the forward (West) FTPC for the three tested event generators (HIJING = solid line, NEXUS = dashed line, VNI = dotted line).*

2.4 Reconstruction of Net Charge Fluctuations

As shown in chapter 1, the excess of positive over negative charges in different regions of phase-space can serve to study the net baryon distribution and, thus, the dynamics of the collision. The experimental challenge in measuring this positive charge excess results from the sensitivity of the signal to possible reconstruction biases. In the acceptance of the FTPC, the net positive charge signal is on the order of 20 tracks in a total of about 500 charged particle tracks per unit of rapidity. Therefore, if only 1% of the reconstructed tracks of one charge are systematically assigned to the other charge, the systematic error introduced is already 25% of the signal.

In the study of the FTPC simulation and analysis software, no indication of systematic biases in the determination of the charge of a reconstructed particle could be found. They are, however, imaginable, especially if the distortion correction for the reconstructed track points has significant errors. The charge assigned to a track is determined from the sign of its curvature in the magnetic field. The magnetic field, however, also influences the electron drift in the FTPC, shifting all points in the same sense in angular direction. The magnitude of this shift is larger for the inner track points than for the outer ones. Therefore, an underestimation of the magnetic field would lead to negative particles being falsely identified as positive, whereas an overestimation of the magnetic field would bias the reconstruction in favor of negative charges. The quality of the distortion correction

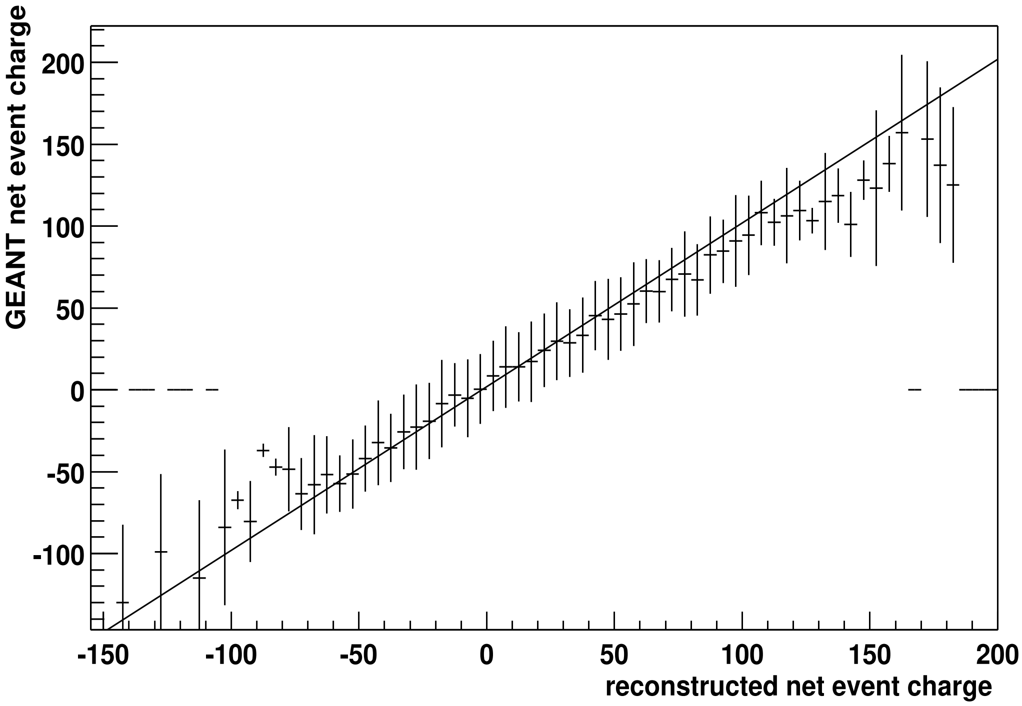

Figure 2.12: *Reconstruction capability for net positive charge per event in the acceptance of the FTPCs. The figure shows the net positive charge per event simulated with GEANT versus the value reconstructed in the FTPC analysis chain. Error bars correspond to the width of the distribution of input values for the respective reconstructed value. The analysis is based upon the reconstruction of approximately 1700 events from the VNI event generator. A diagonal line is included to guide the eye.*

not being known at this point, potential biases from this effect were not included in the present study.

A different source of possible biases in the charge excess measurement are different reconstruction efficiencies for positive and negative charges. The effects of the sector boundaries on the reconstruction of different charges were already mentioned in section 2.1. Another potential bias in the reconstruction efficiency that could be identified and eliminated in the course of this study was linked to the order in which the track finding algorithm searches through the chamber. One angular direction was preferred, so particles of one charge had a higher probability of being reconstructed than particles of the other charge. The problem is now avoided by selecting the angular segments for search in alternating direction.

The above problems will be very difficult to eliminate from measured data for lack of an independent cross-check, which complicates the task of measuring absolute numbers or even spectra of the net positive charge to a reasonable level of certainty. For the measurement of the fluctuations of net positive charge, however, these biases merely shift the center of the distribution, leaving its shape and width nearly unchanged. Consequently, net charge fluctuations are relatively robust against possible biases in either the reconstruction efficiency or the charge measurement.

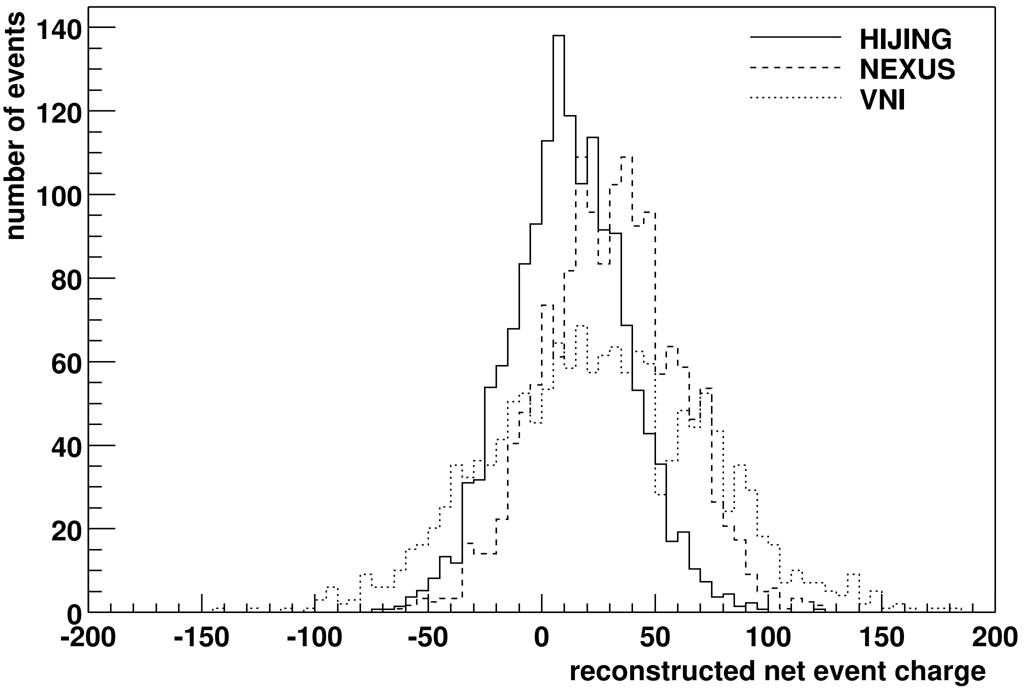

Figure 2.13: *Reconstructed distribution of net positive charges per event in the FTPCs for three different event generators. The solid line shows events from the HIJING event generator, the dashed line from NEXUS and the dotted line from VNI.*

Fluctuations of the net positive charge have become a matter of interest because two recent theoretical publications ([Asa00] and [Jeo00]) suggest a reduction of these fluctuations as a "smoking gun" for quark deconfinement.

Figure 2.12 shows that the reconstructed net positive charge in the FTPCs is linearly connected to the input value of the simulation over a large range of values. Furthermore, the absolute values are reconstructed correctly at least at the present level of simulation, without errors in the distortion correction and with charge-dependent correction parameters derived from simulations of the same event generator. To reduce the contamination from electrons at small transverse momenta and to avoid the very straight tracks at high transverse momenta, where charge identification might have larger uncertainties, the analysis was restricted to measured transverse momenta between 200 MeV/c and 1000 MeV/c.

The net charge distributions (figure 2.13) have a mean value of 11.9 with a standard deviation of 25.3 for HIJING, a mean value of 30.5 with a standard deviation of 28.7 for NEXUS and a mean value of 23.9 with a standard deviation of 47.1 for VNI. The high mean values from NEXUS and VNI and the lower mean value from HIJING are in agreement with what could be expected from figure 1.9. The values are smaller than what might be expected from extrapolating the dN/dy from that figure over the FTPC acceptance because of the restrictive track selection in this analysis. What is more surprising is the large width of fluctuations in VNI, given the fact that both [Asa00] and [Jeo00] suggest a reduction of charge fluctuations in the presence of partonic degrees of freedom. Pure hadron statistics would have suggested similar fluctuations from VNI and NEXUS, as both models have rather similar multiplicities.

This study shows one of the strengths of the large acceptance of the FTPCs in a region of phase space that is expected to contain a large number of baryons. Together with their robustness against reconstruction errors, these results suggest that net charge fluctuations may be one of the most exciting results from the STAR FTPCs that may be available at a very early time in the analysis.

Chapter 3

Summary and Outlook

Rapidity and transverse momentum spectra of different particles from three different simulation algorithms have been compared. Signals which should be accessible to the FTPCs and which should be interesting especially in comparison to the measurements of the TPC at midrapidity include rapidity and transverse momentum spectra of negatively charged hadrons as well as measurements of the excess of positive over negative charges.

Because of their large acceptance, the FTPCs can be used to measure event fluctuations, either independently or in correlation with the TPC. The symmetric detector design also permits the study of forward-backward correlations.

Charged particle multiplicity predictions from different nuclear collision models differ in their mean values but not in the width of their fluctuations. Interesting differences could also be found in the forward-backward correlations of the charged particle multiplicity.

Transverse momentum distributions and their fluctuations can be studied if the correction factors are known to a reasonable level of precision. Model predictions differ more significantly in the mean value than in the fluctuations. Forward-backward correlations in transverse momentum were found to be extremely small.

Net charge fluctuations can be measured even if reconstruction biases can not be ruled out, rendering the mean values unusable. Theoretical publications as well as model predictions let these fluctuations appear to be an especially promising observable.

The STAR FTPCs will be installed in the experiment and ready to take data early in the year 2001. At the planned data taking rate of one event per second, an amount of data comparable to the present study should be available within hours. Without particle identification, rare signals will hardly be accessible to the FTPC. Therefore, most analyses will be possible with relatively modest event numbers. However, except for very robust signals like the charged particle multiplicity or net charge fluctuations, careful studies of the detector performance will have to be done before useful results will be available.

List of Figures

Bibliography

[Asa00] M. Asakawa, U. Heinz and B. Müller, "Fluctuation Probes of Quark deconfinement", hep-ph/0003169, CERN, Geneva (2000)

[Bie98] F. Bieser *et al.*, "The Forward Time Projection Chamber for the STAR Detector", MPI-PhE/98-3, Max-Planck-Institut für Physik, München (1998)

[Dre99] H.J. Drescher *et al.*, "A Unified Treatment of High Energy Interactions", hep-ph/9903296, 9 March 1999

[Gei97] K. Geiger, R. Longacre and D.K. Srivastava, "VNI - Version 4.1 - Simulation of High-Energy Particle Collisions in QCD", Computer Physics Communications 104, 70 (1997)

[Gyu94] M. Gyulassy and X. Wang, "Hijing 1.0: A Monte Carlo Program for Parton and Particle Production in High Energy Hadronic and Nuclear Collisions", Computer Physics Communications 83, 307-331 (1994)

[Hag65] R. Hagedorn, "Statistical Thermodynamics of Strong Interactions at High Energies", Supplemento al Nuovo Cimento III, 2, 147-186 (1965)

[Jeo00] S. Jeon and V. Koch, "Charged Particle Ratio Fluctuation as a Signal for QGP", hep-ph/0003168, Lawrence Berkeley Laboratory, Berkeley (2000)

[Kon97] M. Konrad, "Entwicklung einer hochauflösenden Spurendriftkammer für den Bereich großer Rapidität in Schwerionen-Kollisionen im STAR-Experiment", dissertation, Technische Universität München (1997)